The MHC-E peptide ligands for checkpoint CD94/NKG2A are governed by inflammatory signals, whereas LILRB1/2 receptors are peptide indifferent

Middelburg, J.; Ghaffari, S.; Schoufour, T.A.W.; Sluijter, M.; Schaap, G.; Göynük, B.; ... ; Hall, T. van

Cell Reports

Article

The MHC-E peptide ligands for checkpoint CD94/NKG2A are governed by inflammatory signals, whereas LILRB1/2 receptors are peptide indifferent

Graphical abstract

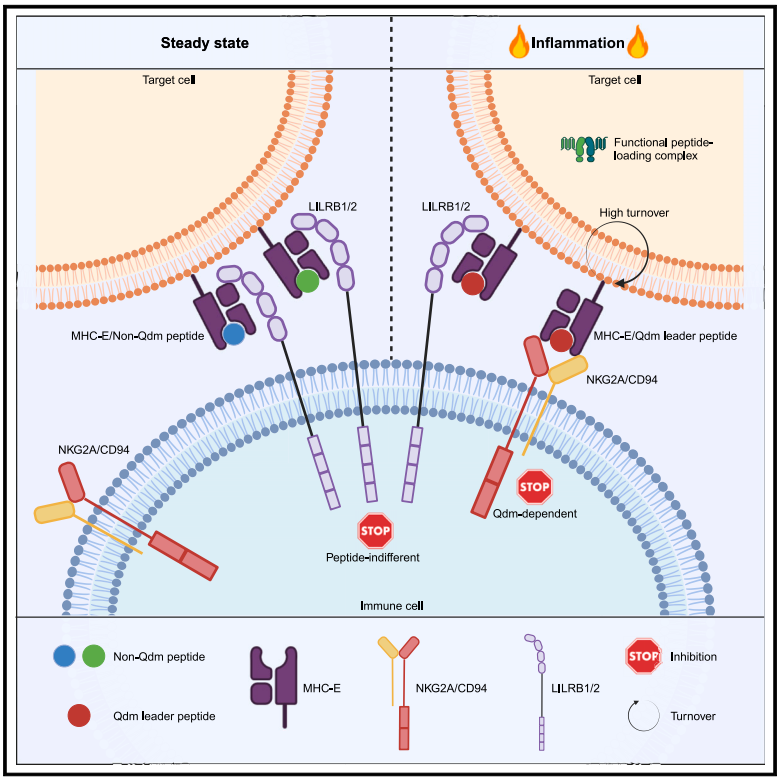

Highlights

- A novel antibody selectively binds to mouse MHC-E (Qa-1^{b}) with Qdm leader peptide
- Qdm peptide presentation requires inflammatory signals and the full peptide-loading complex
- Inhibitory LILRB1/2 receptors engage human MHC-E (HLA-E) irrespective of peptide cargo

Authors

Jim Middelburg, Soroush Ghaffari, Tom A.W. Schoufour, ..., Ruud H.M. Wijdeven, Jon Weidanz, Thorbald van Hall

Correspondence

t.van_hall@lumc.nl

In brief

Middelburg et al. show that the non-classical MHC-E is a central checkpoint ligand for inhibitory receptors on myeloid and lymphoid immunocytes. The LILRB1/2 receptors interact with MHC-E irrespective of the peptide cargo, but the presentation of particular leader peptides, required for CD94/NKG2A interaction, is induced by inflammation.

Middelburg et al., 2023, Cell Reports *42*, 113516
December 26, 2023
https://doi.org/10.1016/j.celrep.2023.113516

CellPress

Cell Reports

CellPress
OPEN ACCESS

Article

The MHC-E peptide ligands for checkpoint CD94/NKG2A are governed by inflammatory signals, whereas LILRB1/2 receptors are peptide indifferent

Jim Middelburg,[1,9] Soroush Ghaffari,[2,9] Tom A.W. Schoufour,[3,9] Marjolein Sluijter,[1] Gaby Schaap,[1] Büsra Göynük,[1] Benedetta M. Sala,[4] Lejla Al-Tamimi,[4] Ferenc Scheeren,[5] Kees L.M.C. Franken,[6] Jimmy J.L.L. Akkermans,[3] Birol Cabukusta,[3] Simone A. Joosten,[6] Ian Derksen,[3] Jacques Neefjes,[3] Sjoerd H. van der Burg,[1] Adnane Achour,[4] Ruud H.M. Wijdeven,[3,10] Jon Weidanz,[7,8,10] and Thorbald van Hall[1,10,11,*]

[1]Department of Medical Oncology, Oncode Institute, Leiden University Medical Center, Leiden, the Netherlands
[2]Department of Biology, College of Science, The University of Texas at Arlington, Arlington, TX, USA
[3]Department of Cell and Chemical Biology, Oncode Institute, Leiden University Medical Center, Leiden, the Netherlands
[4]Science for Life Laboratory, Department of Medicine, Karolinska Institute & Division of Infectious Diseases, Karolinska University Hospital, 171 65 Solna, Sweden
[5]Department of Dermatology, Leiden University Medical Center, Leiden, the Netherlands
[6]Department of Infectious Diseases, Leiden University Medical Center, Leiden, the Netherlands
[7]Abexxa Biologics, Inc., Arlington, TX, USA
[8]College of Nursing and Health Innovation, The University of Texas at Arlington, Arlington, TX, USA
[9]These authors contributed equally
[10]Senior author
[11]Lead contact
*Correspondence: t.van_hall@lumc.nl
https://doi.org/10.1016/j.celrep.2023.113516

SUMMARY

The immune checkpoint NKG2A/CD94 is a promising target for cancer immunotherapy, and its ligand major histocompatibility complex E (MHC-E) is frequently upregulated in cancer. NKG2A/CD94-mediated inhibition of lymphocytes depends on the presence of specific leader peptides in MHC-E, but when and where they are presented *in situ* is unknown. We apply a nanobody specific for the Qdm/Qa-1^b complex, the NKG2A/CD94 ligand in mouse, and find that presentation of Qdm peptide depends on every member of the endoplasmic reticulum-resident peptide loading complex. With a turnover rate of 30 min, the Qdm peptide reflects antigen processing capacity in real time. Remarkably, Qdm/Qa-1^b complexes require inflammatory signals for surface expression *in situ*, despite the broad presence of Qa-1^b molecules in homeostasis. Furthermore, we identify LILRB1 as a functional inhibition receptor for MHC-E in steady state. These data provide a molecular understanding of NKG2A blockade in immunotherapy and assign MHC-E as a convergent ligand for multiple immune checkpoints.

INTRODUCTION

NKG2A is a recently recognized checkpoint in cancer immunity, and therapeutic efficacy of NKG2A-blocking antibodies is currently investigated in clinical trials, including advanced head and neck squamous cell carcinoma, therapy-resistant non-small cell lung cancer, refractory chronic lymphocytic leukemia, and metastatic gastric and colorectal carcinomas.[1,2] The inhibitory receptor NKG2A forms a heterodimeric receptor with CD94 and is selectively expressed on killer lymphocytes, mostly natural killer (NK) cells, γδ T cells, and activated CD8 T cells and is therefore thought to mainly affect cytotoxic activity,[3–7] although NKG2A has recently been reported to promote maintenance of human NK cell expansion capacity.[8] On human γδ T cells, NKG2A expression marks a distinct subset of Vδ2 T cells, exerting strong antitumor effects, which are amplified upon NKG2A blockade.[9] Similarly, we and others previously demonstrated in several preclinical mouse tumor models that NK and CD8 T cells are potentiated by NKG2A blockade, particularly when combined with the widely applied inhibition of the checkpoint PD-1/PD-L1, cancer vaccines, or radiotherapy.[7,10,11] The molecular basis of the limited antitumor efficacy of NKG2A blockade monotherapy is unknown and might be related to its ligand.

NKG2A/CD94 engages the non-classical major histocompatibility complex E (MHC-E) molecules, including HLA-E in humans and Qa-1 in mice, which are characterized by limited polymorphism and low cell surface expression.[12,13] In the worldwide human population, only two HLA-E alleles exist, and these only differ by one amino acid. The overall fold of MHC-E molecules is nearly identical to classical MHC class I, binding non-covalently to the β2m subunit and presenting mostly 9-mer peptides

in their binding groove.[14–16] Interestingly, the germline-encoded NKG2A/CD94 receptor is peptide-specific and docks onto MHC-E/peptide complexes similarly to the T cell receptor (TCR) in a diagonal axis, engaging both the presented peptide as well as MHC-E heavy chain residues localized on the α1 and α2 helices of the peptide binding cleft.[17–21] Leader peptides with the xMAPRTxxL motif, commonly referred to in humans as VML and in mice as Qdm (Qa-1-determinant modifier) are engaged by NKG2A/CD94 and are derived from residues 3–11 of classical MHC-I allotypes.[22] All examined mammalian species contain classical MHC-I allotypes comprising this conserved peptide,[23] pointing to the importance of this receptor-ligand pair in immunity. Indeed, the VML peptide is thought to be constitutively presented under steady state in order to warrant proper NK cell development, education, and tolerance.[24,25] *In vivo* CRISPR screens aiming to identify evasion pathways for immunotherapy recently revealed Qa-1 as an important resistance molecule across different cancer types, underpinning its role in regulating immune responses.[26]

More recently, alternative peptides have been discovered that are capable of efficiently binding to HLA-E but do not contain the VML sequence. These alternative antigens are thought to replace VML/Qdm upon disturbance of homeostasis, but that has never been demonstrated *in situ*. One of such peptides is derived from endogenous HSP60 and another from the viral Nsp13 protein of SARS-CoV-2.[27,28] Interestingly, NKG2A/CD94 does not engage HLA-E when these peptides are presented, allowing activation of NKG2A-expressing effector lymphocytes. In addition, a multitude of antigenic MHC-E-presented peptides have now been identified that trigger TCR-mediated immune responses in the context of autoimmunity, cancer, and pathogenic infections, indicating an adaptive role for MHC-E.[29–31] In the light of this plethora of different peptides, it remains elusive when and where the important VML/Qdm ligand of NKG2A is displayed to the immune system *in situ*. Despite the availability of MHC-E-directed antibodies,[32,33] we still lack tools to specifically detect MHC-E molecules in complex with VML/Qdm peptides.

Here we used our nanobody "EXX1,"[34] which specifically recognizes mouse Qdm/Qa-1^b complexes to provide a mechanistic understanding of why NKG2A functions as a secondary checkpoint. We found that the Qdm peptide is not widely presented by Qa-1^b in homeostasis but is rather induced by inflammatory signals. Moreover, non-Qdm-loaded Qa-1^b molecules are widely present even in the absence of inflammatory signals, and we identified LILRB1 and LILRB2 as MHC-E-binding receptors, irrespective of their peptide cargo. We propose a dual role for MHC-E as checkpoint target for lymphocytes as well as myeloid cells.

RESULTS

EXX1 antibody binds specifically to Qdm/Qa-1^b complexes, whereas 6A8 targets the Qa-1^b heavy chain

To assess when and where different Qa-1^b/peptide complexes are displayed, we used the recently isolated EXX1 nanobody on a mouse IgG2a format, which was raised against recombinant Qdm/Qa-1^b complexes,[34] as well as the commonly used 6A8.6F10.1A6 antibody (hereafter referred to as 6A8). These two antibodies are highly specific for Qa-1^b as confirmed with Qa-1^b knockout (KO) RAW264.7 macrophages and *ex vivo* cultured splenic macrophages from Qa-1^b KO mice (Figure S1A). To test peptide specificity of the EXX1 antibody, we exogenously loaded Qa-1^b-binding peptides Qdm (AMAPRTLLL) and Q001 (AQAERTPEL), a naturally eluted Qa-1^b-binding peptide derived from the DENN domain-containing protein 3, on K562 cells expressing Qa-1^b (Figure 1A). Although Q001-loaded cells resulted in some background staining, EXX1 binding in flow cytometry was predominantly detected for Qdm-loaded K562.Qa-1^b cells, demonstrating its specificity for Qdm, which was in line with the extensive specificity testing reported in our previous work.[34] Of note, this specificity for Qdm is not attributed to a more stable Qa-1^b complex, as the Q001/Qa-1^b complex displayed even higher thermal stability than Qdm/Qa-1^b (Figure S1B). The 6A8 antibody detected Qa-1^b heavy chains even in the absence of these peptides, indicating peptide independency (Figure 1A), which may be expected as 6A8 was raised against a synthetic stretch of the α2 domain of the Qa-1^b heavy chain (Dr. M. Soloski, personal communication) (Figure S1C). As EXX1 distinguished these two peptides differing at four positions (p2, p4, p7, and p8), we assumed that it targeted these unique residues. The crystal structure of Q001/β2m/Qa-1^b complex was determined to 2.4-Å resolution (Table S1) and compared to the previously published crystal structure of the Qdm/β2m/Qa-1^{b}complex (PDB: 3VJ6) (Figures S1C and S1D).[16] These two structures displayed highly similar overall folding, with a root-mean-square value of 0.23 Å for the Cα atoms of heavy chain residues 3–176 (Figure S1D). Comparison of the conformations of peptides Qdm and Q001 demonstrated that they both bind similarly to Qa-1^b (Figure 1B), and that the modification at the anchor position p2 from a methionine in Qdm to a glutamine in Q001 could easily adapt and fit to the requirements of the B-pocket. The three other positions (p4, p7, and p8) that differ between Qdm and Q001 protrude toward the solvent and are all accessible for interactions with EXX1 binding. Importantly, the modifications of the proline (p4) and leucine (p7) residues in Qdm to negatively charged glutamates in Q001 significantly alter the surface charges of these two complexes, increasing the overall electronegativity of the Q001/Qa-1^b surface (Figure 1C). As an additional consequence of the introduction of these two glutamate residues in Q001, the conformation of the side chain of the arginine residue at p5 is slightly altered (Figure 1B). Combined with our previously observed alanine-replacement results in the Qdm peptide,[34] demonstrating loss of binding when peptide residues p3, p6, p7, and p8 were mutated to alanine, these results illustrate that EXX1 is highly specific for the Qdm peptide complexed with Qa-1^b. Thus, EXX1 may be considered a functional NKG2A/CD94 mimic that docks with high specificity to the Qdm/Qa-1^b complex and interacts with several Qdm residues.[18–20]

We then tested whether EXX1 could indeed block interactions between NKG2A/CD94 and Qdm/Qa-1^b (Figure 1D). Tetramers of Qa-1^b containing Qdm or the highly similar Q001 control peptide were used to stain NK cells, freshly isolated from spleens of C57BL/6 mice. While Q001/Qa-1^b tetramers failed to stain NK

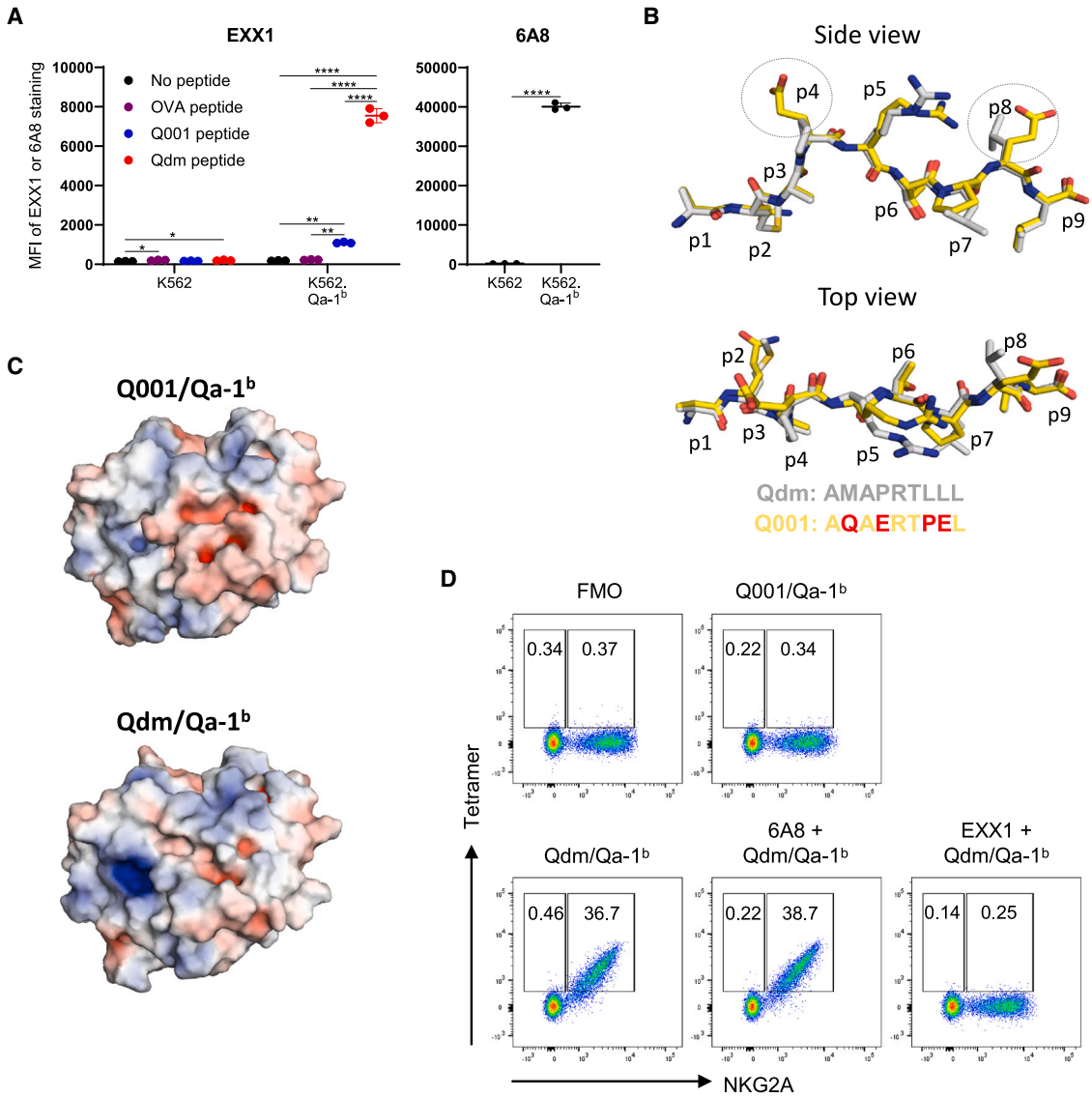

Figure 1. EXX1 antibody specifically binds to the Qdm/Qa-1^b complex

(A) Binding of the EXX1 and 6A8 antibodies to K562 WT or K562.Qa-1^b cells either or not loaded with 100 μg/mL OVA, Q001, or Qdm peptides.

(B) Superposition of Qdm and Q001 peptides represented as sticks from the crystal structures of peptide/Qa-1^b complexes, with Q001 in yellow and Qdm in gray. Qdm/Qa-1^b structure is obtained from the published complex (PDB: 3VJ6).

(C) Top view surface charge representation of peptide/Qa-1^b complexes. Positive surface charges are indicated in blue and negative charges in red. Electrostatic potentials were calculated from the Q001/Qa-1^b complex from this study and the published Qdm/Qa-1^b complex (PDB: 3VJ6).

(D) Binding of Qdm/Qa-1^b or Q001/Qa-1^b tetramers to NK cells from splenocytes, either with or without preincubation with EXX1 antibody prior to staining. Data are represented as mean ± SD for n = 3 (A). Significance was calculated using a two-sided t test (A, 6A8) or using an ANOVA followed by Tukey's post hoc tests comparing all groups (A, EXX1). *p < 0.05, **p < 0.01, ***p < 0.001, and ****p < 0.0001. See also Figure S1 and Table S1.

cells, Qdm/Qa-1^b tetramers selectively stained NKG2A-expressing NK cells. Importantly, preincubation of Qdm/Qa-1^b tetramers with EXX1 antibody prevented interaction with all tested immune cells, confirming EXX1 as a NKG2A/CD94 mimic and a functional blocker of this inhibitory axis. In contrast, 6A8 antibody did not affect NKG2A binding, as it is not specific for the Qdm peptide. Similar data were obtained with bone marrow-isolated NK cells (Figure S1E). These data again illustrate the high specificity of EXX1 to Qdm/Qa-1^b.

Genome-wide CRISPR screens reveal a strong dependency on every member of the peptide loading complex for Qdm presentation

We then applied both antibodies in a genome-wide KO screen to determine essential factors for total Qa-1^b (6A8) and Qdm/Qa-1^b (EXX1) display at the cell surface. For this, a genome-wide clustered regularly interspaced short palindromic repeats (CRISPR)-Cas9 screen was performed in RAW264.7 macrophages (Figure 2A), as these macrophages displayed the highest

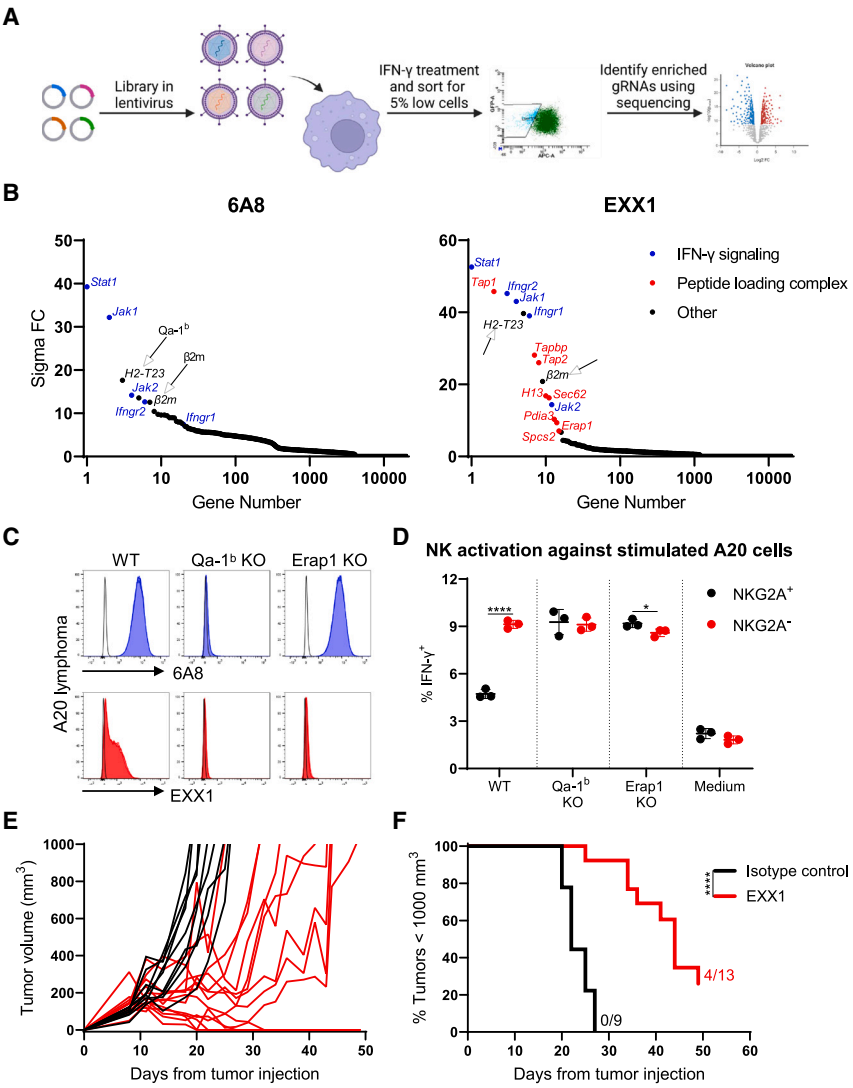

Figure 2. Qdm/Qa-1^b surface display requires a completely functional peptide loading complex

(A) Setup of the genome-wide CRISPR-Cas9 screen for binding of 6A8 and EXX1 antibodies.

(B) Hits of the genetic screens retrieved from the 5% lowest 6A8- or EXX1-binding cells.

(C) Histograms of 6A8 and EXX1 binding to pre-stimulated WT, Qa-1^b KO, or Erap1 KO A20 lymphoma cells. Black open histograms indicate unstained cells.

(D) Reactivity of NKG2A$^+$ or NKG2A$^-$ NK cells isolated from C57BL/6 spleens to pre-stimulated A20 WT, Qa-1^b KO, or Erap1 KO cells.

(E and F) Tumor growth (E) and survival (F) of BALB/c mice that were inoculated with syngeneic A20-eGFP/Fluc tumor cells and treated with EXX1 or isotype control antibodies. Numbers indicate surviving mice at the end of the experiment. Data are represented as mean ± SD of n = 3 (D) or as histograms of a representative experiment of n = 3 (C). Significance was calculated using two-sided t tests (D) or a Mantel-Cox log rank test (F). *p < 0.05, **p < 0.01, ***p < 0.001, and ****p < 0.0001. See also Figure S2 and Tables S2 and S3.

Qdm/Qa-1^b expression. These macrophages were pretreated with IFN-γ to induce high expression of total Qa-1^b and Qdm/Qa-1^b (Figures S2A and S2B), and the lowest 5% of cells were sorted for both antibodies separately. Cells were grown out, and after another sort using the same gating strategy, gRNAs were sequenced and compared to the input. As expected, both screens revealed genes involved in the IFN-γ signal transduction pathway, including *Stat1, Jak1, Jak2,* and both surface receptors for IFN-γ (*Ifngr1* and *Ifngr2*) (Figure 2B; Tables S2 and S3). Furthermore, *β2m* and *H2-T23 (*encoding Qa-1^b) were among the identified essential genes, confirming that both antibodies are selective for Qa-1^b and that binding to Qa-1^b complexes depends on β2m expression in cells. Strikingly, the EXX1 screen yielded all components of the endoplasmic reticulum (ER)-resident peptide-loading complex (PLC) (Figures 2B; Table 1),[35,36] including *Tap1*, *Tap2*, *Tapbp* (encoding tapasin), *Sec62*, *H13* (encoding SPPase), *Pdia3* (encoding ERp57), *Spsc2* (encoding SPase), and *Erap1*, implying that each of these genes were separately essential for surface display of Qdm/Qa-1^b complexes (Figure 2B).

This result demonstrated that presentation of the Qdm peptide by Qa-1^b is a strict reflection of appropriate PLC function. Surprisingly, none of these genes were found in the 6A8 screen, implying that the antigen processing pathway is dispensable for surface display of total Qa-1^b, which is in line with previous findings on stable HLA-E/β2m complexes in the absence of peptide,[37] but contrasting the requirement of peptide loading for surface display of classical MHC-I molecules.[36,38]

We selected the peptide transporter TAP1 and the ER-resident aminopeptidase ERAAP to confirm our findings, since deficiency in these two PLC components was shown by us and others to promote the presentation of an alternative peptide repertoire in Qa-1^b, referred to as TEIPP.[39] gRNAs for TAP1 and ERAAP genes were transduced with Cas9 into A20 and RMA lymphoma lines, B16F10 melanoma, and RAW264.7 macrophages. A complete loss of EXX1 staining was observed in the *Tap1*- and *Erap1*-KO variants, whereas the 6A8 antibody still detected Qa-1^b molecules on these cells (Figures 2C and S2C–S2I). Thus the absence of Qdm through a deficiency in a member of the PLC, such as TAP1, did not result in total loss of Qa-1^b on the cell surface. *Ex vivo* cultured spleen macrophages from *Tap1*$^{-/-}$ and *H2-D*$^{b-/-}$ mice recapitulated these findings (Figure S2J). Although these latter mice harbor a functional PLC, they lack the Qdm leader peptide that is derived from the classical MHC class I protein H-2D^b in C57BL/6 mice. Alternatively, Qdm is indirectly involved in EXX1 binding, similar to what was found for Mamu-E-restricted T cell responses in non-human primate studies.[40] We concluded that these data confirmed our observation that EXX1 recognition is strictly dependent on the

Table 1. PLC gene hits from a genome-wide CRISPR-Cas9 screen using EXX1

Gene name	Protein name	Function
Tap1	TAP1	transports short peptides from cytosol to ER. Forms a heterodimer with TAP2
Tap2	TAP2	transports short peptides from cytosol to ER. Forms a heterodimer with TAP1
Tapbp	TAP binding protein/tapasin	mediates interaction between MHC heavy chain and TAP and chaperones peptide loading
H13	SPPase (signal peptide peptidase)	endopeptidase liberating signal peptides from the ER membrane
Sec62	Sec62	channel for translocation of nascent proteins into the ER
Spcs2	SPase (signal peptidase)	cleaves signal peptides from nascent proteins in the ER
Pdia3	ERp57	chaperone folding and processing of nascent MHC class I in the ER
Erap1	Erap1/ERAAP	aminopeptidase that trims peptides in the ER for binding to MHC class I

TAP, transporter associated with antigen processing; ER, endoplasmic reticulum.

presence of the Qdm peptide in the Qa-1^b cleft and that this presence requires a functional PLC.

Since lymphocytes are only impaired in their effector response when NKG2A/CD94 engages Qdm/Qa-1^b complexes on target cells, but not with Qa-1^b loaded with other peptides, we hypothesized that NKG2A$^+$ NK cells are not impaired upon interaction with ERAAP-deficient target cells, as they lack presentation of Qdm. To test this hypothesis, panels of Qa-1^b- or ERAAP-KO A20 lymphoma and RAW264.7 cells were tested for recognition *in vitro* by freshly isolated NK cells from allogeneic C57BL/6 spleens (Figures 2D and S2K). Recognition of WT target cells was significantly lower in NKG2A$^+$ NK cells compared to the NKG2A$^-$ subset in the population. However, NKG2A$^+$ NK cells were not inhibited in their recognition of ERAAP-KO target cells, despite similar surface levels of total Qa-1^b, defined by 6A8 antibody binding (Figures 2C, 2D, S2C, S2F, S2K, and S2I). Similar results were obtained for Qa-1^b KO target cells, limiting potential confounding factors that are co-expressed with NKG2A. Thus, NKG2A-mediated effector cell inhibition specifically depends on Qdm/Qa-1^b complexes and not total Qa-1^b surface levels. After showing the strict Qdm peptide dependency for NKG2A-mediated inhibition, we used this NK cell activation assay to determine Qdm peptide presentation in Qa-1^b on unstimulated RAW264.7 cells (Figures S2A and S2B). The reactivity of NKG2A$^+$ and NKG2A$^-$ NK subsets was similar, however not completely equal, to unstimulated WT target cells, indicating that very low levels of Qdm/Qa-1^b complexes might exist in the absence of interferon (Figures S2L and S2M). Finally, we tested the therapeutic potential of the NKG2A-mimicking antibody EXX1 in a preclinical mouse tumor model. BALB/c mice, which also encode the Qa-1^b allotype, were inoculated with syngeneic A20 lymphoma cells and treated with EXX1 antibody or an isotype control when tumors were palpable. Treatment with the EXX1 antibody significantly delayed tumor outgrowth and improved survival (Figures 2E and 2F), demonstrating the therapeutic potential of targeting the NKG2A ligand Qdm/Qa-1^b via EXX1, in addition to previously reported NKG2A blocking antibodies.[7,10] Altogether, these results indicate that (1) Qdm presentation is strictly dependent on a fully functional PLC, (2) the 6A8 antibody does not discriminate among the peptide cargo in Qa-1^b, and (3) the EXX1 antibody can be used for therapeutic applications.

Qdm presentation reflects recent IFN-γ signaling and real-time supply of newly formed Qdm/Qa-1^b complexes

The cells used for the aforementioned analyses were all pretreated with IFN-γ to induce high surface levels of Qa-1^b complexes. We next studied the effects of IFN-γ stimulation on the expression levels of critical factors that we have identified (Figure 2B) for Qdm/Qa-1^b presentation. Therefore, quantitative rtPCR assays were performed on transcriptomes of B16F10 melanoma, A20 lymphoma, and RAW264.7 macrophages (Figure 3A). *Stat1*, used as a positive control, showed a clear upregulation in all three cell lines following IFN-γ pretreatment. *β2m*, *H2-T23* (Qa-1^b), and PLC members *Tap1*, *Tap2*, *Erap1*, and *Tapbp* (tapasin) were strongly upregulated by IFN-γ, while transcripts for the Sec62 channel, the SPPase enzyme, and the ERp57 disulfide isomerase were not influenced by IFN-γ. Interestingly, cell surface expression of the Qa-1^b heavy chain (*H2-T23*) in B16F10 tumor cells was upregulated by a notable 5,000-fold, suggesting a highly sensitive STAT1-mediated activation of the gamma-interferon activation site.[41] Qa-1^b induction was strongest in B16F10 melanoma cells as expression levels in the hematopoietic cell lines RAW264.7 and A20 were already higher at baseline (Figure S3A). Given the overlap between genes required for Qdm loading and classical MHC-I peptide loading, Qdm presentation by Qa-1^b apparently reflects the efficiency of the antigen presentation capacity of cells.

Next, we studied the durability of an IFN-γ pulse on Qa-1^b surface expression, as this cytokine is mostly present *in vivo* during temporal inflammatory responses.[42] RAW264.7 and B16F10 cells were incubated for 48 h with IFN-γ and washed before further culture in normal medium for up to 24 h (Figure 3B). Cell surface levels of Qa-1^b and classical H-2L^d (on RAW264.7) or H-2D^b (on B16F10), detected by the 28.14.8S antibody, were stable for at least 6 h after removal of IFN-γ (Figures 3C and S3B). However, 24 h after removal of IFN-γ, total Qa-1^b and Qdm/Qa-1^b complexes decreased by 40% on both cell lines (Figure 3C). In contrast, surface levels of H-2L^d/H-2D^b complexes remained stable on both cell lines. These findings indicate that, in contrast to classical MHC class I molecules, presentation

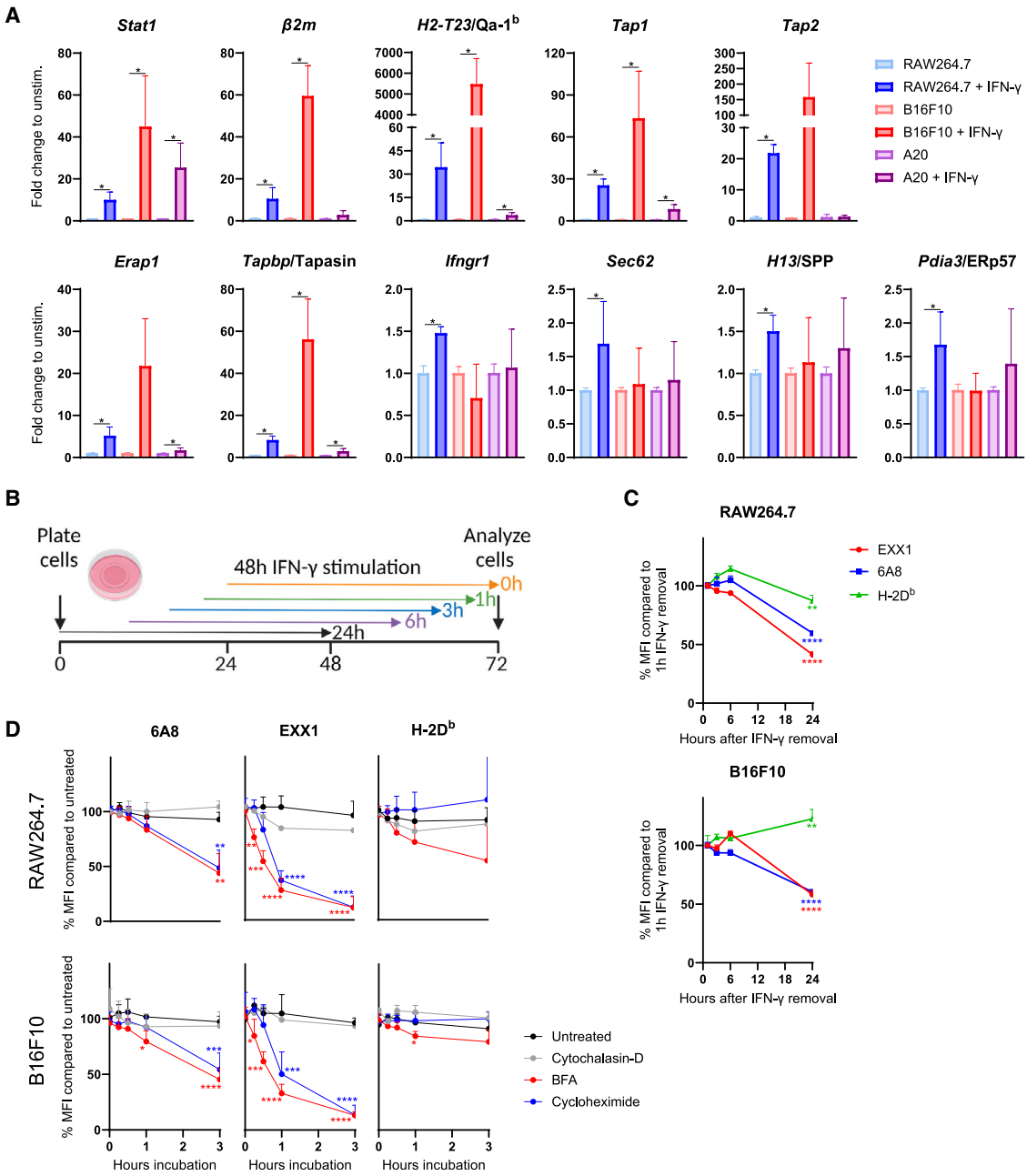

Figure 3. Qdm/Qa-1^b is a real-time sensor for functional antigen presentation machinery

(A) Effect of IFN-γ stimulation on gene expression of RAW264.7, B16F10, and A20 cells by RT-PCR analysis.

(B and C) Setup (B) and data (C) for analysis of total Qa-1^b (6A8), Qdm/Qa-1^b (EXX1), and H-2D^b expression on RAW264.7 and B16F10 cells after 2 days pre-treatment of cells with 5 IU/mL or 30 IU/mL IFN-γ, respectively, followed by washing away IFN-γ for the remainder of the 3-day experimental time frame. Statistics are shown for the 24-h time point.

(D) Decay of surface proteins for total Qa-1^b (6A8), Qdm/Qa-1^b (EXX1), and H-2D^b on pre-stimulated RAW264.7 and B16F10 cells in the presence of indicated inhibitors. Data are represented as mean ± SD of n = 4 (A), n = 3 (C), or n = 2–6 (D). Significance was calculated using Wilcoxon signed rank tests (A) or one-way ANOVA followed by Dunnett post-hoc tests compared to 1 h (C) or untreated (D). *p <0.05, **p < 0.01, ***p < 0.001, and ****p < 0.0001. See also Figure S3.

of total Qa-1^b and Qdm/Qa-1^b complexes requires recent IFN-γ signaling.

We therefore investigated whether the dynamics in Qdm/Qa-1^b staining reflected only transcriptional activity or also involved protein stability of Qdm/Qa-1^b complexes. Surface Qa-1^b decay values were measured using the protein synthesis inhibitor cycloheximide and the "Golgi transport inhibitor" brefeldin A (BFA) (Figure 3D). Cells were sampled after different time points and

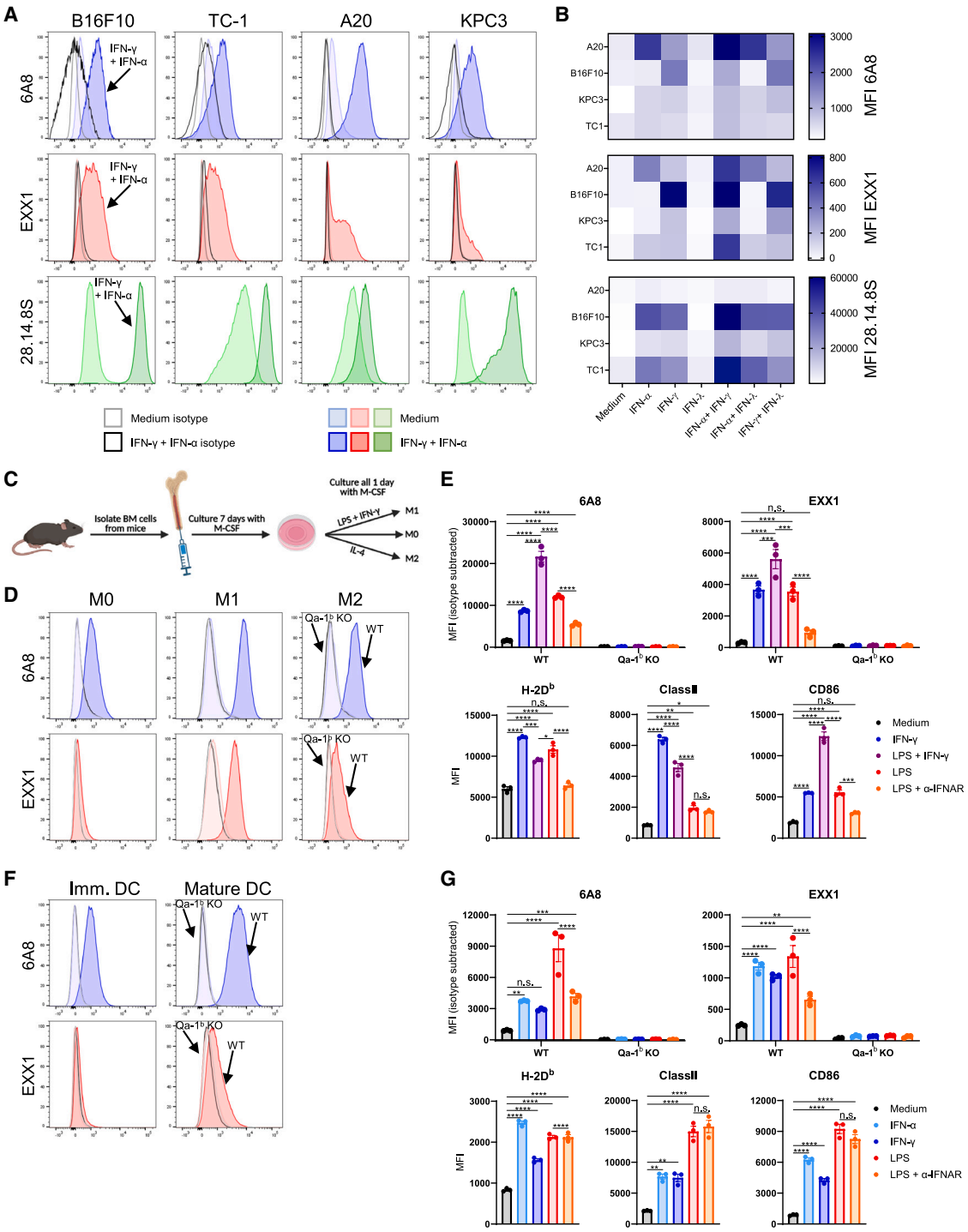

Figure 4. Expression of Qdm/Qa-1^b is induced by inflammatory signals, including interferons and TLR agonists

(A) Expression of total Qa-1^b (6A8), Qdm/Qa-1^b (EXX1), and H-2D^b (28.14.8S) on B16F10, TC-1, A20, and KPC3 tumor cells following 2 days of stimulation with 30 IU/mL IFN-γ and 10,000 IU/mL IFN-α.

(B) Expression of total Qa-1^b (6A8), Qdm/Qa-1^b (EXX1), and H-2D^b (28.14.8S) for B16F10, KPC3, and TC1 or H-2L^d (28.14.8S) for A20 on tumor cells following 2 days of stimulation with single or combination treatments of 10,000 IU/mL IFN-α, 30 IU/mL IFN-γ, and 20 ng/mL IFN-λ.

(C) Flow scheme for the generation of bone marrow-derived macrophages (BMDMs).

(D) Histograms showing 6A8 and EXX1 binding to M0, M1, or M2 BMDMs. Gray open histograms: unstained Qa-1^b KO BMDMs; black open histograms: unstained WT BMDMs; filled light histograms: stained Qa-1^b KO BMDMs; filled dark histograms: stained WT BMDMs.

(legend continued on next page)

decay values of total Qa-1^b (6A8), Qdm/Qa-1^b complexes (EXX1), total H-2L^d/H-2D^b, and PD-L1 molecules as controls were calculated. The half-life of Qdm/Qa-1^b complexes was surprisingly short, close to 30 min (Figures 3D and S3C–S3M). BFA was slightly more efficient than cycloheximide, possibly due to a small set of molecules in transit to the cell surface when treatment was initiated. The total amount of Qa-1^b complexes, as detected by the 6A8 antibody, was significantly more stable compared to Qdm/Qa-1^b complexes, with a half-life of approximately 3 h. Finally, no decay of H-2L^d/H-2D^b nor PD-L1 cell surface expression was detected within this time frame. Inhibition with the proteasome inhibitor marizomib also decreased Qdm/Qa-1^b surface levels (Figures S3D, S3E, S3H, and S3J), albeit considerably more slowly, which likely reflects the involvement of the proteasome in the liberation of the Qdm epitope from nascent MHC-I molecules or other cellular effects following long-term proteasome inhibition.[43,44] Inhibition of endocytosis by an effective concentration of the actin-disrupting drug cytochalasin-D (Figure S3N) did not affect cell surface expression levels and also failed to prevent the decay of Qa-1^b molecules in the presence of BFA or cycloheximide (Figures 3D and S3C–S3M), indicating that the short half-life of Qdm/Qa-1^b complexes was not the result of common endocytosis. Altogether, these results indicate that Qdm/Qa-1^b complexes have a high cell surface turnover and can thus be considered a real-time sensor for optimal PLC-mediated antigen processing and presentation.

Type I/II interferons and TLR ligands induce Qdm/Qa-1^b cell surface expression

Thus far, we have studied Qdm/Qa-1^b expression following stimulation with IFN-γ. Next, we extended this for other proinflammatory stimuli, such as type I and III interferons, which are produced by more tissues than the immune system-restricted type II interferon IFN-γ. We tested whether these broadly released cytokines were also capable of inducing Qdm presentation (Figures 4A, 4B, and S4A). A panel of four murine tumor cell lines (A20 lymphoma, B16F10 melanoma, KPC3 pancreatic ductal adenocarcinoma, and HPV16-transformed TC1 cells) were incubated with each of these three different interferons or with a mix of two types together. Treatment with IFN-α (type I) strongly induced Qdm/Qa-1^b expression on A20 lymphoma cells and to a lower extent also on TC1. Interestingly, treatment with IFN-γ (type II) resulted in the strongest Qdm/Qa-1^b induction on all solid tumor cell lines, especially when combined with IFN-α (type I). In contrast, effects of IFN-λ stimulation (type III) were minimal and were only observed in the pancreas carcinoma cell line KPC3 when combined with IFN-γ (Figures 4B and S4A).

Then, *ex vivo* cultured bone marrow-derived macrophages (BMDMs) and dendritic cells (BMDCs) were tested with interferon and toll-like receptor (TLR) ligands. TLRs signal through nuclear factor-kappa B (NF-κB), thereby promoting immune responses through differentiation and maturation of macrophages and dendritic cells.[45] Therefore, TLR ligands are frequently used as adjuvants in vaccines.[46] Bone marrow precursors from WT or Qa-1^b KO mice were cultured in the presence of macrophage colony-stimulating factor (M-CSF) for 7 days, after which the macrophages were differentiated overnight to M1 or M2 types (Figure 4C). M1-type macrophages, differentiated with the combination of lipopolysaccharide (LPS) and IFN-γ, expressed inducible nitric oxide synthase (iNOS), CD86, and PD-L1, while M2-type macrophages, differentiated with IL-4, displayed an increased expression of early growth response 2 (Egr2), whereas M0 macrophages displayed low expression levels for all these markers (Figure S4B).[47] Strikingly, Qdm/Qa-1^b complexes were not present on M0 macrophages as assessed by EXX1 staining, while presence of Qa-1^b was unambiguously determined through staining with 6A8 (Figure 4D). In contrast, proinflammatory M1-type macrophages displayed high surface levels of Qdm/Qa-1^b following overnight incubation with LPS and IFN-γ. To determine which of these two factors was most influential, we tested the effects of each one alone and found that the effects of the TLR4 ligand LPS were comparable to IFN-γ (Figures 4E and S4C). Nevertheless, a combination of LPS and IFN-γ resulted in the highest expression of Qdm/Qa-1^b, total Qa-1^b, and CD86.

Bone marrow precursors were then cultured in the presence of granulocyte macrophage colony-stimulating factor (GM-CSF) and IL-4 to generate dendritic cells, and we matured these BMDCs in the presence of LPS, IFN-α, or IFN-γ. The inflammatory components LPS, IFN-α, or IFN-γ induced maturation of the BMDCs, indicated by enhanced expression of CD86 and MHC class II molecules and concomitantly Qdm/Qa-1^b complexes (Figures 4F, 4G, S4D, and S4E). In contrast to M0 macrophages, immature BMDCs did express low levels of Qdm/Qa-1^b complexes together with total Qa-1^b (6A8), although these were strongly boosted following stimulation. Release of interferons by macrophages and DCs upon NF-κB activation has been described and is an efficient way to amplify inflammatory signals, also in an autocrine way.[48] Therefore, we stimulated BMDMs and BMDCs with LPS in the presence of blocking antibodies for type I IFN receptor (IFNAR). A reduction in the Qdm/Qa-1^b surface expression was observed upon addition of these blocking antibodies, suggesting

(E) Expression of total Qa-1^b (6A8), Qdm/Qa-1^b (EXX1), H-2D^b, class II, and CD86 by BMDMs stimulated for 1 day with single or combination treatments of 100 ng/mL LPS, 20 IU/mL IFN-γ, and 20 μg/mL IFNAR blocking antibodies after 7 days of culture with M-CSF. mean fluorescence intensity (MFI) values of isotype stainings for 6A8 and EXX1 were subtracted from the MFI values of the complete staining.

(F) Histograms showing 6A8 and EXX1 binding to unstimulated or matured (1 day with 100 ng/mL LPS) bone marrow-derived DC (BMDC). Histogram colors are as in (D).

(G) Expression of total Qa-1^b (6A8), Qdm/Qa-1^b (EXX1), H-2D^b, class II, and CD86 by BMDMs that have been stimulated for 1 day with 100 ng/mL LPS, 20 IU/mL IFN-γ, 10,000 IU/mL IFN-α, or 20 μg/mL IFNAR blocking antibodies after 7 days of culture with GM-CSF and IL-4. MFI values of isotype staining for 6A8 and EXX1 were subtracted from the MFI values of the complete staining. Data are represented as mean ± SEM of n = 4 (E and G) or as histograms or heatmaps for representative experiments of n = 1 (A, B, D, and F). Significance was calculated using one-way ANOVA followed by Tukey post hoc tests comparing all groups (E and G), and significance is only shown for comparisons of interest. *$p < 0.05$, **$p < 0.01$, ***$p < 0.001$, and ****$p < 0.0001$. Comparisons between medium conditions of WT and Qa-1^b KO mice for 6A8 and EXX1 staining yielded the following p values: (E) 6A8 p = 0.297, EXX1 p = 0.999; (G) 6A8 p = 0.869, EXX1 p = 0.368. See also Figure S4.

that a proportion of LPS-induced Qdm/Qa-1^b expression was mediated via autocrine interferon signaling (Figures 4E and 4G). In assembly, these data suggest that the Qdm peptide is not presented on differentiated macrophages and minimally on DCs, despite the abundance of Qa-1^b molecules on their cell surfaces, and that presence of Qdm is strictly induced by proinflammatory stimuli, predominantly by type I and II interferons and to a lesser extent by TLR agonists such as LPS.

In homeostasis, Qdm is only detected on pDCs despite common surface expression of Qa-1^b heavy chain

The absence of Qdm/Qa-1^b complexes on cultured macrophages and minimal expression on DCs was unexpected, since it is generally assumed that Qdm is presented in homeostasis. To corroborate our findings, we provoked inflammation in naive C57BL/6 mice using tilorone as an interferon inducer,[49] CD40 agonistic antibody,[50] or immunotherapy protocols for the treatment of B16F10 melanoma and TC1 tumors. The applied immunotherapy protocols were previously developed and led to intratumoral infiltration of activated T cells and partial tumor control (Figures S5A–S5D).[51,52] Spleens and tumors were dispersed and stained with panels of antibodies in order to distinguish several lymphoid and myeloid cell lineages. Examples of 6A8 and EXX1 staining on CD4 T cells, classical macrophages, and plasmacytoid DCs (pDCs) from naive wild-type and Qa-1^b-deficient mice are shown in Figure 5A. Steady-state expression levels of total Qa-1^b complexes were low but detectable on all cell types in naive mice (Figures 5A, 5B, and S6A). In contrast, Qdm/Qa-1^b complexes were selectively present on pDCs, which are known for their potent production of type I IFN,[53] albeit at low levels. All inflammatory signals boosted total Qa-1^b expression on all cell types, while the interferon inducer tilorone promoted Qdm peptide presentation most significantly. In general, Qdm presentation was predominantly increased during these treatments on several myeloid cells including macrophages, conventional DC populations cDC1 and cDC2, as well as monocyte-derived dendritic cells (Figures 5B and S6). Altogether, these findings demonstrate that, in contrast to the general assumption, Qdm is not commonly presented by Qa-1^b in steady state *in vivo*, but it requires inflammatory conditions in order to be expressed on the cell surface. Conversely, these data imply that other Qa-1^b complexes are present on cell surfaces under homeostatic conditions.

MHC-E acts as an inhibitory ligand for LILRB1-expressing myeloid cells in a peptide-independent manner and impairs phagocytic uptake

Given that Qa-1^b is commonly expressed in homeostasis but does not contain Qdm and thus will not engage the NKG2A/CD94 inhibitory receptor, we wondered whether MHC-E has additional binding receptors. To identify these, we performed a genome-wide CRISPR activation screen that induces expression of single genes from host cells. Since this library was only available for the human genome, we transduced human K562 cells and stained these cells with a pool of four different HLA-E tetramers, containing the VML leader peptide (VMAPRTLIL) and three other HLA-E stabilizing peptides (VLRPGGHFL, RMPPLGHEL, and RLPAKAPLL), in order to screen in a peptide-independent way. Cells that labeled positive for HLA-E were sorted out, and gRNAs were sequenced to determine the binding receptor (Figure 6A). Both replicates unambiguously identified leukocyte immunoglobulin-like receptor B1 (LILRB1) and LILRB2 (Figure 6B; Table S4). To validate this result, K562.LILRB1 and K562.LILRB2 cells were generated using activating gRNA or using cDNAs, and they were stained with HLA-E tetramers containing the VMAPRTLIL (VML) peptide or the VLRPGGHFL (VLR) peptide derived from *Mycobacterium tuberculosis*[54] (Figures 6C, S7A, and S7B). LILRB1- as well as LILRB2-expressing cells, but not parental K562 cells, efficiently bound both tetramers, indicating that interaction with HLA-E was peptide independent. In contrast, K562.NKG2A/CD94-transfected cells selectively bound the HLA-E/VML complex (Figure 6D), in line with our data in the mouse system. The interaction between LILRB1 and HLA-E tetramers was then further confirmed using co-immunoprecipitation, indicating a direct interaction (Figure S7C). To map the expression of LILRB1 on PBMCs from healthy donors, we performed spectral flow cytometry profiling with 21 markers to determine cell lineages (Figures 6E, 6F, and S7D). LILRB1 was not detected on T cells or NK cells, and only low expression levels were present on B cells. However, lineages from the myeloid compartment, particularly monocytes, cDCs, and pDCs, expressed high levels of LILRB1.

Indeed, previous literature described LILRB1 as an inhibitory checkpoint for macrophages, binding to classical HLA class I molecules,[55] implying that the contribution of HLA-E in the context of total HLA class I expression had to be assessed. First, LILRB1- and LILRB2-transduced J774 mouse macrophages were co-cultured with fluorescently labeled WT, HLA-E KO, or total HLA class I KO Raji target cells, and cell-cell adhesion was subsequently measured (Figure S7E). LILRB1 or LILRB2 expression was unambiguously required for adhesion to Raji target cells and was significantly lower for HLA-E KO Raji cells. Cell adhesion returned to baseline levels after removal of all HLA class I molecules. This Raji panel was then incubated with 2B4-LILRB1 reporter cells, which express GFP upon triggering via LILRB1 (Figures 6G–6I). In line with the adhesion assay, LILRB1 signaling was significantly lower for HLA-E KO Raji cells compared to WT cells and completely returned to baseline levels for total HLA class I KO Raji cells. Importantly, removal of HLA-E did not reduce the total HLA class I staining, as measured by the W6/32 antibody that also binds HLA-E, indicating that absence of HLA-E is sensed by LILRB1 despite normal expression of the classical alleles. Finally, we performed phagocytosis assays using monocyte-derived macrophages (moDMs) to determine the functional consequence of HLA-E engagement. K562 target cells were transfected with HLA-E and co-cultured with moDMs (Figures S7F and S7G). HLA-E expression inhibited phagocytic uptake of K562 target cells, and this impairment was clearer in the presence of blocking antibodies to the "don't eat me" checkpoint CD47 (Figure 6J).[56] These findings were recapitulated in the mouse system, where BMDMs were co-cultured with B16.Qa-1^{b+} or B16.Qa-1^{b-} target cells, in the presence of TA99 as an opsonizing antibody (Figure 6K).[57] Altogether, these results indicate that MHC-E functionally acts as a phagocytic inhibitor for myeloid cells, irrespective of the peptide cargo.

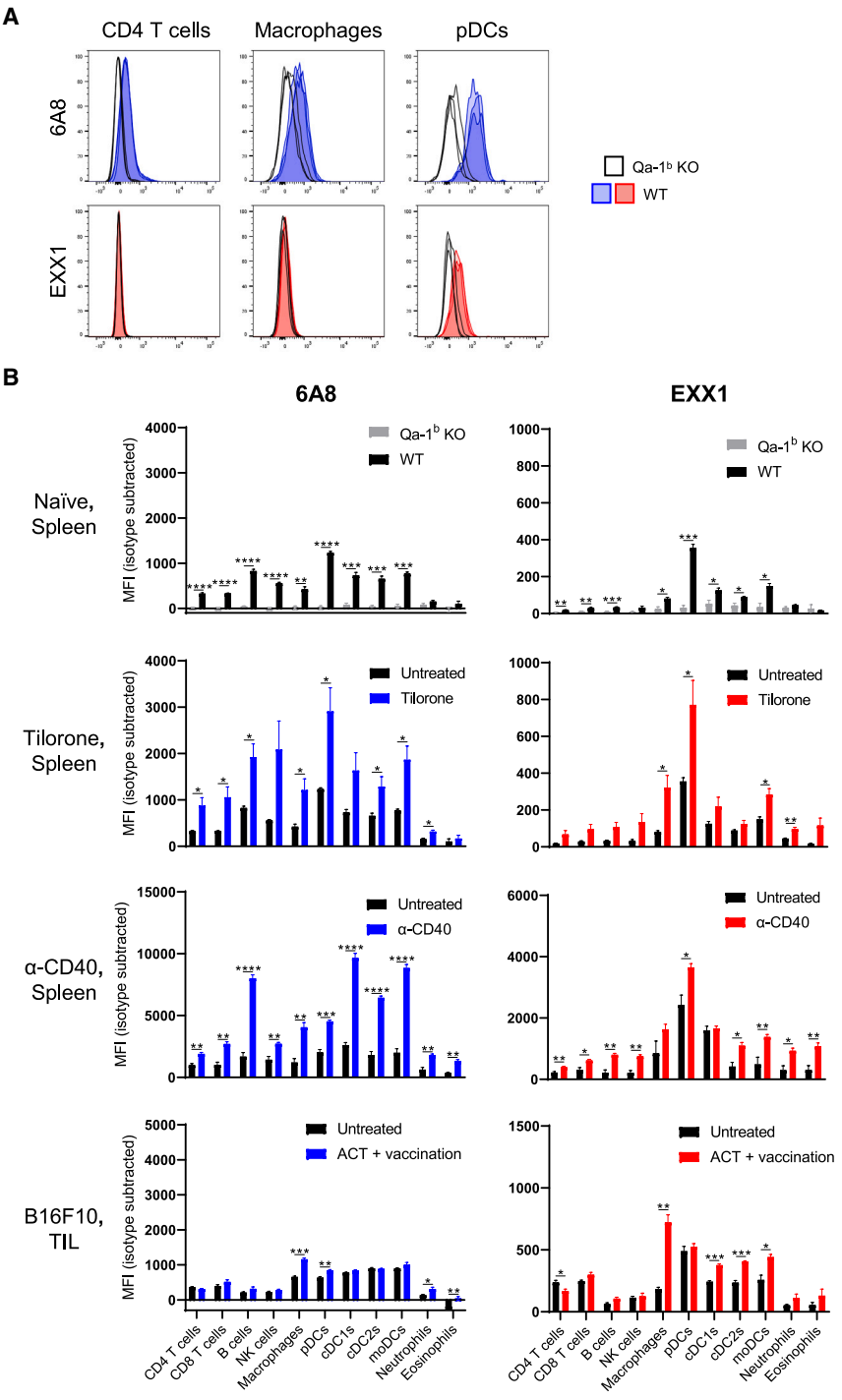

Figure 5. Qdm is selectively presented by Qa-1^b in the presence of inflammatory responses

(A) Flow cytometry staining of total Qa-1^b (6A8) and Qdm/Qa-1^b (EXX1) on CD4 T cells, macrophages, and pDCs from spleens of naive WT or Qa-1^b KO mice.

(B) Quantified results on immune cells from spleens or tumors of mice receiving indicated treatments. MFI values of isotype stainings for 6A8 and EXX1 were subtracted from the MFI values of the complete stainings. Data are represented as mean ± SEM of n = 3–4 (B) or as histograms for n = 3 (A). Significance was calculated using two-sided t tests (B). *p < 0.05, **p < 0.01, ***p < 0.001, and ****p < 0.0001. See also Figures S5 and S6.

DISCUSSION

Here, we used our recently developed antibody EXX1 to study the expression of the NKG2A ligand Qdm/Qa-1^b complex to gain more insight in the function and relevance of this lymphocyte checkpoint and to guide future therapeutic applications. Interestingly, we found that the Qdm peptide is not presented by Qa-1^b on the cell surface under homeostatic conditions, despite presence of Qa-1^b heavy chains, but requires inflammatory signals. Our findings contrast the general assumption in the field that Qdm is the dominant peptide in Qa-1^b molecules. This contrast is likely explained by the fact that the previous studies commonly used LPS-stimulated lymphoblasts to detect Qdm peptide,[58–60] resulting in Qdm presentation. The requirement of inflammatory conditions for expression of Qdm/Qa-1^b is in line with previous findings demonstrating that protection of normal as well as transformed target cells against NK cell lysis was mediated via interferons.[61] Additionally, several publications have described interferons as mediators of immunotherapy resistance in cancer and pointed to Qa-1^b as a major player.[26,62,63] Furthermore, interruption of the NKG2A/CD94-MHC-E interaction led to improved outcomes of immunotherapy only when combined with PD-1/PD-L1 blockade, cancer vaccines, or radiotherapy, which all induce inflammatory responses.[7,10] Our findings provide a mechanistic understanding why NKG2A functions as a secondary checkpoint, because the ligand is selectively expressed under inflammatory conditions.

The highly limited presence of Qdm under homeostatic conditions, with maybe the exception of type I IFN-producing pDCs, may initiate rethinking on NKG2A/CD94 in relation to the education and licensing models of NK cells.[24,25,64,65] Education models assume involvement of NKG2A/CD94 engagement with Qdm/Qa-1^b complexes during hematopoiesis and that these interactions improve the functional capacity of NK cells as adult cells. Although education has been clearly shown for killer cell immunoglobulin-like receptors in general and for NKG2A on uterine NK cells, where IFN-γ is present for remodeling of the uterine

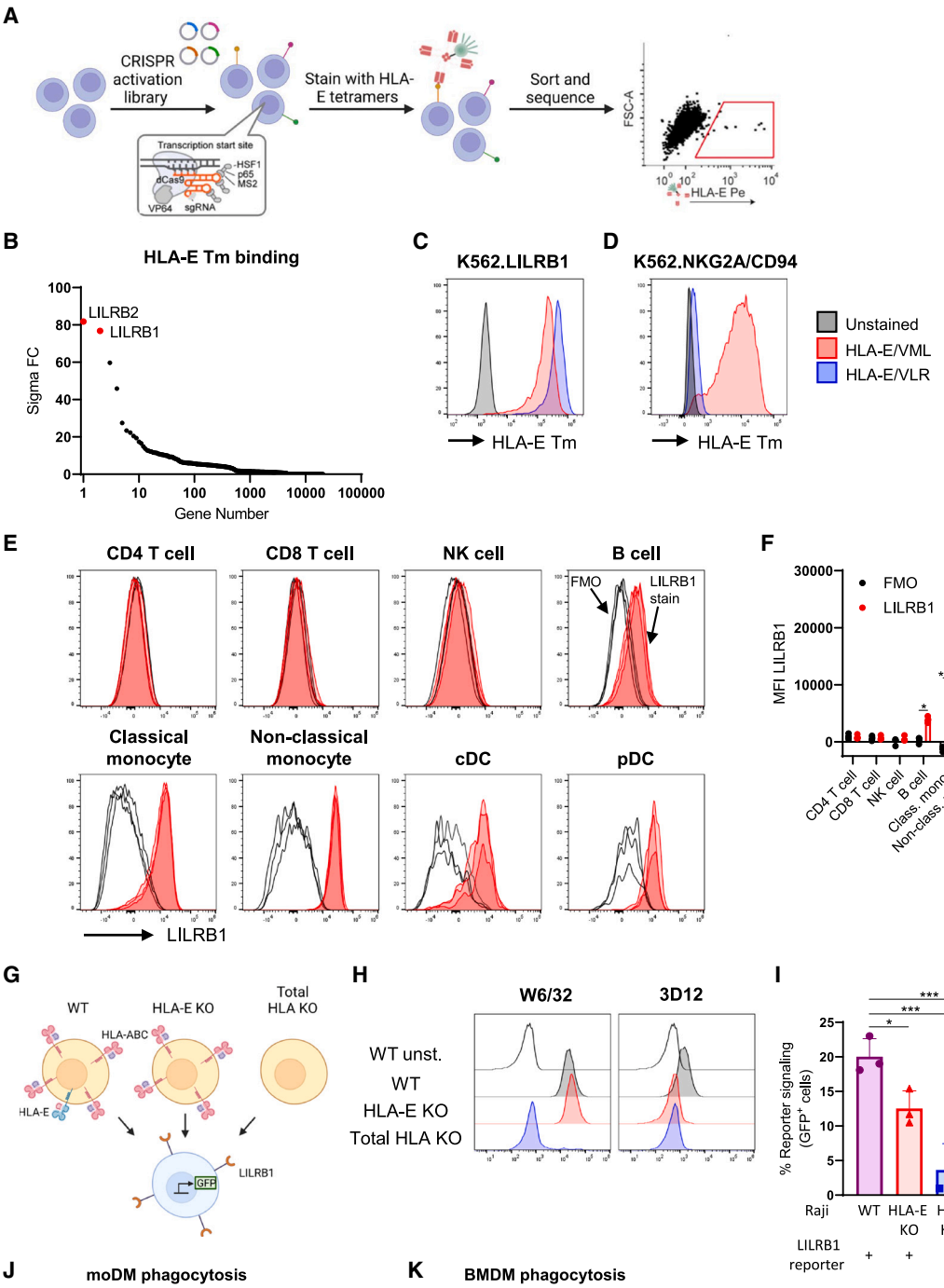

(legend on next page)

arteries,[66] the involvement of the NKG2A receptor is in our opinion much less convincing given the minimal expression of its ligand in steady-state conditions.[24,25,65] Thus, we postulate that NKG2A/CD94 might rather be regarded as a negative feedback receptor after immune activation, instead of a steady-state signaling threshold controller.[67]

The role of this checkpoint under acute inflammatory conditions is underpinned by the half-life of Qdm/Qa-1^b complexes of only 30 min, which is very short compared to other MHC class I molecules that reportedly display half-lives of several hours up to single days.[68] Recombinant Qdm/Qa-1^b complexes were also found to be very unstable at 37°C in contrast to classical H-2K^b/SIINFEKL complexes.[69] This suggests that the short half-life of Qdm/Qa-1^b is most likely an intrinsic feature of this complex even though our thermal stability study revealed a melting temperature of 50.5°C. As Qdm presentation by Qa-1^b depended on every member of the PLC (Figure 2), this real-time sensor is capable to quickly report jeopardizing actions by intracellular pathogens. Interestingly, multiple viruses,[70] as well as cancers,[71] have been described to evade patrolling CD8 T cells by inhibiting the antigen presentation machinery, mostly by dysregulation of TAP proteins. This results in decrease of viral antigen presentation, which can already be detected within 30 min following infection,[72] as well as failure to present Qdm peptide, allowing NK cell and T cell activation due to lack of NKG2A/CD94 signaling. The finding that all studied mammalian MHC-E molecules coexist with other MHC class I alleles coding for a leader peptide with Qdm/VML motif underscores the importance of this control mechanism.[23]

Intriguingly, antigen-presenting cells, such as DCs and macrophages, display high levels of Qa-1^b heavy chains on the cell surface and are expected to have sufficient levels of these PLC components for efficient loading of Qa-1^b, but they still show minimal presentation of Qdm without inflammatory signals. Moreover, the Qdm-donating molecule H-2D^b is also not limiting, considering its cell surface display and our CRISPR screen even identified alternative Qdm-donor genes *H2-Q8* (coding for Qa-2) and *H2-Q10*, implying the presence of sufficient intracellular Qdm peptide. We speculate that either a specific inflammation-inducible factor is required for Qdm/Qa-1^b expression or that a yet unknown protein prevents the Qdm peptide from loading into Qa-1^b, even in situations where the entire PLC is intact. An alternative option is that in DCs other peptides outcompete the Qdm peptide for loading onto Qa-1^b, but it is unclear whether this is the case. Interestingly, the readily detected Qa-1^b heavy chains were presented independently from the PLC in RAW264.7 macrophages, which is in contrast to classical MHC class I molecules,[36] thereby warranting further research into the peptide content and pathways for these Qa-1^b complexes. The intracellular processing for MHC-E peptide loading was previously reported to deviate from that of classical MHC class I; e.g., recirculation via endolysosomes has been demonstrated in macrophages.[40,73] Whether the classical peptide loading of HLA-E is exclusive or whether multiple pathways for MHC-E peptide loading exist is yet to be determined.

In a CRISPR activation screen, we identified the two homologous molecules LILRB1 and LILRB2 as binders of HLA-E. The binding of LILRB1 and LILRB2 molecules to HLA-E is in line with previous studies, which reported the molecular interaction between LILRB1 and various classical HLA class I molecules *in vitro* and showed that LILRB1 docks onto β2m and the α3 domain of HLA class I.[55,74,75] This binding site does not involve direct contacts with the peptide accommodated in the binding groove, thereby perfectly agreeing with our observation that LILRB1 showed binding to HLA-E, irrespective of peptide cargo. We especially observed LILRB1 expression on monocytes and DCs in PBMCs from healthy donors, which is in line with previous reports that describe LILRB1 as a "don't eat me" receptor on macrophages by impairing phagocytosis of target cells through interaction with classical HLA class I molecules.[55,76,77] Our data suggest a higher affinity of LILRB1 for HLA-E than other HLA molecules, since loss of HLA-E impacted LILRB1 signaling in the presence of normal levels of classical alleles. We speculate that induction of MHC-E on target cells leads to decreased target cell killing by myeloid cell-mediated phagocytosis and potentially also reduced antigen presentation and priming of T cell responses. Interestingly, in our previous work, we observed stronger antitumor effects when we used Qa-1^b KO tumors than with NKG2A blocking antibodies,[7] hinting to a broader role for MHC-E in antitumor immunity than just acting as a ligand for NKG2A. The relative contribution of NKG2A as a lymphocytic checkpoint compared to LILRB1 on myeloid cells remains to be determined in further investigations exploiting LILRB1 in tumor immunity in context with MHC-E.

Altogether, we have provided a mechanistic understanding regarding the functioning of NKG2A/MHC-E as a secondary

Figure 6. HLA-E induces inhibitory LILRB1 signaling and dampens phagocytosis

(A) Setup of a genome-wide CRISPR activation screen using a pool of four HLA-E tetramers.

(B) Hits of the genetic screen retrieved from the HLA-E tetramer-positive cells.

(C and D) Histograms showing binding of HLA-E tetramers containing the VML leader peptide or VLR MTub-derived peptide to K562 cells expressing LILRB1 (C) or NKG2A/CD94 (D).

(E and F) LILRB1 flow cytometry staining on immune cell subsets from PBMCs of healthy donors displayed as histograms (E) or bar graphs (F).

(G) Setup of reporter assay for LILRB1 signaling, using 2B4-LILRB1 reporter cells and a panel of Raji target cells. LILRB1 signaling results in expression of GFP.

(H) Histograms showing expression of total HLA class I (W6/32) and HLA-E (3D12) on the Raji panel.

(I) Reporter assay showing LILRB1 signaling or background signaling.

(J) Phagocytosis assay using M1-differentiated human monocyte-derived macrophages and CFSE-labeled K562.HLA-E$^+$ or K562.HLA-E$^-$ cells.

(K) Phagocytosis assay using M1-differentiated BMDMs and pre-stimulated CFSE-labeled B16.Qa-1^{b+} or B16.Qa-1^{b-} cells. Data are represented as mean ± SD of n = 3–4 (F and I–K) or as histograms from a representative experiment of three independent experiments n = 1 (C, D, and H) or n = 3 (E). Significance was calculated using paired two-sided t tests (F), an ANOVA followed by Dunnett's post hoc tests compared to WT (I), or unpaired two-sided t tests (J and K). *p < 0.05, **p <0.01, ***p < 0.001, and ****p < 0.0001. See also Figure S7 and Table S4.

immune checkpoint upon the presence of inflammatory responses and showed an additional inhibitory function via LILRB1, thereby providing a framework for how to target MHC-E in future immunotherapy approaches.

Limitations of the study

In this study, we have primarily investigated MHC-E in the mouse (Qdm/Qa-1^b complexes), as a specific antibody for human VML/HLA-E complexes is not yet available. Once available, it will be important to verify our findings to the human setting of HLA-E. Regarding our Qdm/Qa-1^b targeting antibody EXX1, we did observe some background binding to the highly homologous peptide Q001 at high concentrations, and despite extensive specificity studies in this and our previous paper,[34] we formally cannot exclude some reactivity to alternative peptide/Qa-1^b complexes. Furthermore, our NK activation assay revealed that there might be very low levels of Qdm/Qa-1^b present on the cell surface of cells in the absence of inflammatory signals, which were too low for EXX1 binding. However, we anticipate that the functional consequences of these low levels will be limited given the relatively small effect on NK cell inhibition. Finally, we have not yet identified the receptor responsible for inhibition of phagocytic activity in mouse macrophages, although paired immunoglobulin-like receptor-B (PIR-B) is a likely candidate.

STAR★METHODS

Detailed methods are provided in the online version of this paper and include the following:

SUPPLEMENTAL INFORMATION

Supplemental information can be found online at https://doi.org/10.1016/j.celrep.2023.113516.

ACKNOWLEDGMENTS

We thank our colleagues Saskia Santegoets, Lisa Griffioen, Anouk Stolk, Linda de Bruin, Ziena Abdulrahman, and David van Gijlswijk for access to human materials and input regarding the human flow cytometry panels. We thank Anneloes van Duijn for her input and materials regarding the LILRB1 section. Furthermore, we thank our colleagues from the flow cytometry facility, animal facility, and peptide facility of the LUMC. Finally, graphics were created with BioRender.com. This research was supported by collaborative grants from Abexxa Biologics and Boehringer Ingelheim to T.v.H. and J.W., by a research grant from the Nederlandse Organisatie voor Wetenschappelijk Onderzoek (NWO, ICI00021) to J.N., and by research grants from the Swedish Cancer Society (21 1605 Pj01H), Swedish Research Council (2021-05061), and Cancer- och Allergifonden (10399) to A.A.

AUTHOR CONTRIBUTIONS

Conceptualization: J.M., S.G., T.A.W.S., R.H.M.W., J.W., and T.v.H.; methodology: J.N., A.A., R.H.M.W., J.W., and T.v.H.; formal analysis: J.M., S.G., T.A.W.S., M.S., G.S., B.G., B.M.S., L.A.-T., and R.H.M.W.; investigation: J.M., S.G., T.A.W.S., M.S., G.S., B.G., B.M.S., L.A.-T., and R.H.M.W.; resources: F.S., K.L.M.C.F., S.A.J., I.D., J.J.L.L.A., and B.C.; writing – original draft: J.M. and T.v.H.; writing – review & editing: J.M., A.A., S.H.v.d.B., R.H.M.W., J.W., and T.v.H.; supervision: A.A., S.H.v.d.B., R.H.M.W., J.W., and T.v.H.; funding acquisition: J.N., A.A., J.W., and T.v.H.

DECLARATION OF INTERESTS

J.W. was co-founder and chief scientist at Abexxa Biologics, Inc., during the study and had ownership interest (including stock and patents) of Abexxa. J.W. is a consultant for Boehringer-Ingelheim International GmbH. T.v.H. reports receiving a commercial grant from Abexxa and was an advisory board member for the same.

INCLUSION AND DIVERSITY

We support inclusive, diverse, and equitable conduct of research.

Received: June 13, 2023
Revised: September 23, 2023
Accepted: November 14, 2023
Published: December 3, 2023

REFERENCES

1. Borst, L., van der Burg, S.H., and van Hall, T. (2020). The NKG2A-HLA-E Axis as a Novel Checkpoint in the Tumor Microenvironment. Clin. Cancer Res. *26*, 5549–5556.
2. Herbst, R.S., Majem, M., Barlesi, F., Carcereny, E., Chu, Q., Monnet, I., Sanchez-Hernandez, A., Dakhil, S., Camidge, D.R., Winzer, L., et al. (2022). COAST: An Open-Label, Phase II, Multidrug Platform Study of Durvalumab Alone or in Combination With Oleclumab or Monalizumab in Patients With Unresectable, Stage III Non-Small-Cell Lung Cancer. J. Clin. Oncol. *40*, 3383–3393.
3. Borst, L., Sluijter, M., Sturm, G., Charoentong, P., Santegoets, S.J., van Gulijk, M., van Elsas, M.J., Groeneveldt, C., van Montfoort, N., Finotello,

F., et al. (2022). NKG2A is a late immune checkpoint on CD8 T cells and marks repeated stimulation and cell division. Int. J. Cancer *150*, 688–704.

4. Kamiya, T., Seow, S.V., Wong, D., Robinson, M., and Campana, D. (2019). Blocking expression of inhibitory receptor NKG2A overcomes tumor resistance to NK cells. J. Clin. Invest. *129*, 2094–2106.
5. Abd Hamid, M., Wang, R.-Z., Yao, X., Fan, P., Li, X., Chang, X.-M., Feng, Y., Jones, S., Maldonado-Perez, D., Waugh, C., et al. (2019). Enriched HLA-E and CD94/NKG2A Interaction Limits Antitumor CD8(+) Tumor-Infiltrating T Lymphocyte Responses. Cancer Immunol. Res. *7*, 1293–1306.
6. van Hall, T., André, P., Horowitz, A., Ruan, D.F., Borst, L., Zerbib, R., Narni-Mancinelli, E., van der Burg, S.H., and Vivier, E. (2019). Monalizumab: inhibiting the novel immune checkpoint NKG2A. J. Immunother. cancer *7*, 263.
7. van Montfoort, N., Borst, L., Korrer, M.J., Sluijter, M., Marijt, K.A., Santegoets, S.J., van Ham, V.J., Ehsan, I., Charoentong, P., André, P., et al. (2018). NKG2A Blockade Potentiates CD8 T Cell Immunity Induced by Cancer Vaccines. Cell *175*, 1744–1755.e15.
8. Kaulfuss, M., Mietz, J., Fabri, A., Vom Berg, J., Münz, C., and Chijioke, O. (2023). The NK cell checkpoint NKG2A maintains expansion capacity of human NK cells. Sci. Rep. *13*, 10555.
9. Cazzetta, V., Bruni, E., Terzoli, S., Carenza, C., Franzese, S., Piazza, R., Marzano, P., Donadon, M., Torzilli, G., Cimino, M., et al. (2021). NKG2A expression identifies a subset of human Vδ2 T cells exerting the highest antitumor effector functions. Cell Rep. *37*, 109871.
10. André, P., Denis, C., Soulas, C., Bourbon-Caillet, C., Lopez, J., Arnoux, T., Bléry, M., Bonnafous, C., Gauthier, L., Morel, A., et al. (2018). Anti-NKG2A mAb Is a Checkpoint Inhibitor that Promotes Anti-tumor Immunity by Unleashing Both T and NK Cells. Cell *175*, 1731–1743.e13.
11. Battaglia, N.G., Murphy, J.D., Uccello, T.P., Hughson, A., Gavras, N.W., Caldon, J.J., Gerber, S.A., and Lord, E.M. (2022). Combination of NKG2A and PD-1 Blockade Improves Radiotherapy Response in Radioresistant Tumors. J. Immunol. *209*, 629–640.
12. Hermel, E., Hart, A.J., Gunduz, I., Acton, H., Kim, C., Wurth, M., Uddin, S., Smith, C., Fischer Lindahl, K., and Aldrich, C.J. (2004). Polymorphism and conservation of the genes encoding Qa1 molecules. Immunogenetics *56*, 639–649.
13. Brochu, H., Wang, R., Tollison, T., Pyo, C.-W., Thomas, A., Tseng, E., Law, L., Picker, L.J., Gale, M., Jr., Geraghty, D.E., and Peng, X. (2022). Alternative splicing and genetic variation of mhc-e: implications for rhesus cytomegalovirus-based vaccines. Commun. Biol. *5*, 1387.
14. O'Callaghan, C.A., Tormo, J., Willcox, B.E., Braud, V.M., Jakobsen, B.K., Stuart, D.I., McMichael, A.J., Bell, J.I., and Jones, E.Y. (1998). Structural features impose tight peptide binding specificity in the nonclassical MHC molecule HLA-E. Mol. Cell *1*, 531–541.
15. Ying, G., Wang, J., Kumar, V., and Zajonc, D.M. (2017). Crystal structure of Qa-1a with bound Qa-1 determinant modifier peptide. PLoS One *12*, e0182296.
16. Zeng, L., Sullivan, L.C., Vivian, J.P., Walpole, N.G., Harpur, C.M., Rossjohn, J., Clements, C.S., and Brooks, A.G. (2012). A structural basis for antigen presentation by the MHC class Ib molecule, Qa-1b. J. Immunol. *188*, 302–310.
17. Sullivan, L.C., Clements, C.S., Beddoe, T., Johnson, D., Hoare, H.L., Lin, J., Huyton, T., Hopkins, E.J., Reid, H.H., Wilce, M.C.J., et al. (2007). The heterodimeric assembly of the CD94-NKG2 receptor family and implications for human leukocyte antigen-E recognition. Immunity *27*, 900–911.
18. Kaiser, B.K., Pizarro, J.C., Kerns, J., and Strong, R.K. (2008). Structural basis for NKG2A/CD94 recognition of HLA-E. Proc. Natl. Acad. Sci. USA *105*, 6696–6701.
19. Petrie, E.J., Clements, C.S., Lin, J., Sullivan, L.C., Johnson, D., Huyton, T., Heroux, A., Hoare, H.L., Beddoe, T., Reid, H.H., et al. (2008). CD94-NKG2A recognition of human leukocyte antigen (HLA)-E bound to an HLA class I leader sequence. J. Exp. Med. *205*, 725–735.
20. Kraft, J.R., Vance, R.E., Pohl, J., Martin, A.M., Raulet, D.H., and Jensen, P.E. (2000). Analysis of Qa-1(b) peptide binding specificity and the capacity of CD94/NKG2A to discriminate between Qa-1-peptide complexes. J. Exp. Med. *192*, 613–624.
21. Ruibal, P., Derksen, I., van Wolfswinkel, M., Voogd, L., Franken, K.L.M.C., El Hebieshy, A.F., van Hall, T., Schoufour, T.A.W., Wijdeven, R.H., Ottenhoff, T.H.M., et al. (2023). Thermal-exchange HLA-E multimers reveal specificity in HLA-E and NKG2A/CD94 complex interactions. Immunology *168*, 526–537.
22. Braud, V., Jones, E.Y., and McMichael, A. (1997). The human major histocompatibility complex class Ib molecule HLA-E binds signal sequence-derived peptides with primary anchor residues at positions 2 and 9. Eur. J. Immunol. *27*, 1164–1169.
23. Kurepa, Z., Hasemann, C.A., and Forman, J. (1998). Qa-1b binds conserved class I leader peptides derived from several mammalian species. J. Exp. Med. *188*, 973–978.
24. Raulet, D.H. (2006). Missing self recognition and self tolerance of natural killer (NK) cells. Semin. Immunol. *18*, 145–150.
25. Elliott, J.M., and Yokoyama, W.M. (2011). Unifying concepts of MHC-dependent natural killer cell education. Trends Immunol. *32*, 364–372.
26. Manguso, R.T., Pope, H.W., Zimmer, M.D., Brown, F.D., Yates, K.B., Miller, B.C., Collins, N.B., Bi, K., LaFleur, M.W., Juneja, V.R., et al. (2017). In vivo CRISPR screening identifies Ptpn2 as a cancer immunotherapy target. Nature *547*, 413–418.
27. Michaëlsson, J., Teixeira de Matos, C., Achour, A., Lanier, L.L., Kärre, K., and Söderström, K. (2002). A signal peptide derived from hsp60 binds HLA-E and interferes with CD94/NKG2A recognition. J. Exp. Med. *196*, 1403–1414.
28. Hammer, Q., Dunst, J., Christ, W., Picarazzi, F., Wendorff, M., Momayyezi, P., Huhn, O., Netskar, H.K., Maleki, K.T., García, M., et al. (2022). SARS-CoV-2 Nsp13 encodes for an HLA-E-stabilizing peptide that abrogates inhibition of NKG2A-expressing NK cells. Cell Rep. *38*, 110503.
29. Hansen, S.G., Wu, H.L., Burwitz, B.J., Hughes, C.M., Hammond, K.B., Ventura, A.B., Reed, J.S., Gilbride, R.M., Ainslie, E., Morrow, D.W., et al. (2016). Broadly targeted $CD8^+$ T cell responses restricted by major histocompatibility complex E. Science *351*, 714–720.
30. Ottenhoff, T.H.M., and Joosten, S.A. (2019). Mobilizing unconventional T cells. Science *366*, 302–303.
31. van Hall, T., Oliveira, C.C., Joosten, S.A., and Ottenhoff, T.H.M. (2010). The other Janus face of Qa-1 and HLA-E: diverse peptide repertoires in times of stress. Microbes Infect. *12*, 910–918.
32. Li, D., Brackenridge, S., Walters, L.C., Swanson, O., Harlos, K., Rozbesky, D., Cain, D.W., Wiehe, K., Scearce, R.M., Barr, M., et al. (2022). Mouse and human antibodies bind HLA-E-leader peptide complexes and enhance NK cell cytotoxicity. Commun. Biol. *5*, 271.
33. Ravindranath, M.H., Filippone, E.J., Devarajan, A., and Asgharzadeh, S. (2019). Enhancing Natural Killer and CD8(+) T Cell-Mediated Anticancer Cytotoxicity and Proliferation of CD8(+) T Cells with HLA-E Monospecific Monoclonal Antibodies. Monoclon. Antib. Immunodiagn. Immunother. *38*, 38–59.
34. Ghaffari, S., Upchurch-Ange, K., Gimlin, S., Tripathi, T., Sluijter, M., Middelburg, J., van Hall, T., and Weidanz, J. (2022). A Single-Domain TCR-like Antibody Selective for the Qa-1(b)/Qdm Peptide Complex Enhances Tumoricidal Activity of NK Cells via Blocking the NKG2A Immune Checkpoint. J. Immunol. *208*, 2246–2255.
35. Thomas, C., and Tampé, R. (2021). MHC I assembly and peptide editing - chaperones, clients, and molecular plasticity in immunity. Curr. Opin. Immunol. *70*, 48–56.
36. Blees, A., Januliene, D., Hofmann, T., Koller, N., Schmidt, C., Trowitzsch, S., Moeller, A., and Tampé, R. (2017). Structure of the human MHC-I peptide-loading complex. Nature *551*, 525–528.

37. Walters, L.C., Harlos, K., Brackenridge, S., Rozbesky, D., Barrett, J.R., Jain, V., Walter, T.S., O'Callaghan, C.A., Borrow, P., Toebes, M., et al. (2018). Pathogen-derived HLA-E bound epitopes reveal broad primary anchor pocket tolerability and conformationally malleable peptide binding. Nat. Commun. *9*, 3137.

38. Wearsch, P.A., and Cresswell, P. (2008). The quality control of MHC class I peptide loading. Curr. Opin. Cell Biol. *20*, 624–631.

39. Oliveira, C.C., van Veelen, P.A., Querido, B., de Ru, A., Sluijter, M., Laban, S., Drijfhout, J.W., van der Burg, S.H., Offringa, R., and van Hall, T. (2010). The nonpolymorphic MHC Qa-1b mediates CD8+ T cell surveillance of antigen-processing defects. J. Exp. Med. *207*, 207–221.

40. Verweij, M.C., Hansen, S.G., Iyer, R., John, N., Malouli, D., Morrow, D., Scholz, I., Womack, J., Abdulhaqq, S., Gilbride, R.M., et al. (2021). Modulation of MHC-E transport by viral decoy ligands is required for RhCMV/SIV vaccine efficacy. Science *372*, eabe9233.

41. Au-Yeung, N., Mandhana, R., and Horvath, C.M. (2013). Transcriptional regulation by STAT1 and STAT2 in the interferon JAK-STAT pathway. JAK-STAT *2*, e23931.

42. Hoekstra, M.E., Bornes, L., Dijkgraaf, F.E., Philips, D., Pardieck, I.N., Toebes, M., Thommen, D.S., van Rheenen, J., and Schumacher, T.N.M. (2020). Long-distance modulation of bystander tumor cells by CD8(+) T cell-secreted IFNγ. Nat. cancer *1*, 291–301.

43. Bland, F.A., Lemberg, M.K., McMichael, A.J., Martoglio, B., and Braud, V.M. (2003). Requirement of the proteasome for the trimming of signal peptide-derived epitopes presented by the nonclassical major histocompatibility complex class I molecule HLA-E. J. Biol. Chem. *278*, 33747–33752.

44. Dantuma, N.P., Groothuis, T.A.M., Salomons, F.A., and Neefjes, J. (2006). A dynamic ubiquitin equilibrium couples proteasomal activity to chromatin remodeling. J. Cell Biol. *173*, 19–26.

45. Kawai, T., and Akira, S. (2007). Signaling to NF-kappaB by Toll-like receptors. Trends Mol. Med. *13*, 460–469.

46. Duthie, M.S., Windish, H.P., Fox, C.B., and Reed, S.G. (2011). Use of defined TLR ligands as adjuvants within human vaccines. Immunol. Rev. *239*, 178–196.

47. Jablonski, K.A., Amici, S.A., Webb, L.M., Ruiz-Rosado, J.d.D., Popovich, P.G., Partida-Sanchez, S., and Guerau-de-Arellano, M. (2015). Novel Markers to Delineate Murine M1 and M2 Macrophages. PLoS One *10*, e0145342.

48. Richez, C., Yasuda, K., Watkins, A.A., Akira, S., Lafyatis, R., van Seventer, J.M., and Rifkin, I.R. (2009). TLR4 ligands induce IFN-alpha production by mouse conventional dendritic cells and human monocytes after IFN-beta priming. J. Immunol. *182*, 820–828.

49. Ekins, S., Lingerfelt, M.A., Comer, J.E., Freiberg, A.N., Mirsalis, J.C., O'Loughlin, K., Harutyunyan, A., McFarlane, C., Green, C.E., and Madrid, P.B. (2018). Efficacy of Tilorone Dihydrochloride against Ebola Virus Infection. Antimicrob. Agents Chemother. *62*, e01711-17.

50. van Mierlo, G.J.D., den Boer, A.T., Medema, J.P., van der Voort, E.I.H., Fransen, M.F., Offringa, R., Melief, C.J.M., and Toes, R.E.M. (2002). CD40 stimulation leads to effective therapy of CD40(-) tumors through induction of strong systemic cytotoxic T lymphocyte immunity. Proc. Natl. Acad. Sci. USA *99*, 5561–5566.

51. Beyranvand Nejad, E., Labrie, C., Abdulrahman, Z., van Elsas, M.J., Rademaker, E., Kleinovink, J.W., van der Sluis, T.C., van Duikeren, S., Teunisse, A.F.A.S., Jochemsen, A.G., et al. (2020). Lack of myeloid cell infiltration as an acquired resistance strategy to immunotherapy. J. Immunother. cancer *8*, e001326.

52. Ly, L.V., Sluijter, M., Versluis, M., Luyten, G.P.M., van Stipdonk, M.J., van der Burg, S.H., Melief, C.J.M., Jager, M.J., and van Hall, T. (2010). Peptide vaccination after T-cell transfer causes massive clonal expansion, tumor eradication, and manageable cytokine storm. Cancer Res. *70*, 8339–8346.

53. Zhou, B., Lawrence, T., and Liang, Y. (2021). The Role of Plasmacytoid Dendritic Cells in Cancers. Front. Immunol. *12*, 749190.

54. Joosten, S.A., van Meijgaarden, K.E., van Weeren, P.C., Kazi, F., Geluk, A., Savage, N.D.L., Drijfhout, J.W., Flower, D.R., Hanekom, W.A., Klein, M.R., and Ottenhoff, T.H.M. (2010). Mycobacterium tuberculosis peptides presented by HLA-E molecules are targets for human CD8 T-cells with cytotoxic as well as regulatory activity. PLoS Pathog. *6*, e1000782.

55. Barkal, A.A., Weiskopf, K., Kao, K.S., Gordon, S.R., Rosental, B., Yiu, Y.Y., George, B.M., Markovic, M., Ring, N.G., Tsai, J.M., et al. (2018). Engagement of MHC class I by the inhibitory receptor LILRB1 suppresses macrophages and is a target of cancer immunotherapy. Nat. Immunol. *19*, 76–84.

56. Logtenberg, M.E.W., Scheeren, F.A., and Schumacher, T.N. (2020). The CD47-SIRPα Immune Checkpoint. Immunity *52*, 742–752.

57. Andrechak, J.C., Dooling, L.J., Tobin, M.P., Zhang, W., Hayes, B.H., Lee, J.Y., Jin, X., Irianto, J., and Discher, D.E. (2022). CD47-SIRPα Checkpoint Disruption in Metastases Requires Tumor-Targeting Antibody for Molecular and Engineered Macrophage Therapies. Cancers *14*, 1930.

58. Aldrich, C.J., DeCloux, A., Woods, A.S., Cotter, R.J., Soloski, M.J., and Forman, J. (1994). Identification of a Tap-dependent leader peptide recognized by alloreactive T cells specific for a class Ib antigen. Cell *79*, 649–658.

59. Cotterill, L.A., Stauss, H.J., Millrain, M.M., Pappin, D.J., Rahman, D., Canas, B., Chandler, P., Stackpoole, A., Simpson, E., Robinson, P.J., and Dyson, P.J. (1997). Qa-1 interaction and T cell recognition of the Qa-1 determinant modifier peptide. Eur. J. Immunol. *27*, 2123–2132.

60. DeCloux, A., Woods, A.S., Cotter, R.J., Soloski, M.J., and Forman, J. (1997). Dominance of a single peptide bound to the class I(B) molecule, Qa-1b. J. Immunol. *158*, 2183–2191.

61. Malmberg, K.-J., Levitsky, V., Norell, H., de Matos, C.T., Carlsten, M., Schedvins, K., Rabbani, H., Moretta, A., Söderström, K., Levitskaya, J., and Kiessling, R. (2002). IFN-gamma protects short-term ovarian carcinoma cell lines from CTL lysis via a CD94/NKG2A-dependent mechanism. J. Clin. Invest. *110*, 1515–1523.

62. Benci, J.L., Johnson, L.R., Choa, R., Xu, Y., Qiu, J., Zhou, Z., Xu, B., Ye, D., Nathanson, K.L., June, C.H., et al. (2019). Opposing Functions of Interferon Coordinate Adaptive and Innate Immune Responses to Cancer Immune Checkpoint Blockade. Cell *178*, 933–948.e14.

63. Benci, J.L., Xu, B., Qiu, Y., Wu, T.J., Dada, H., Twyman-Saint Victor, C., Cucolo, L., Lee, D.S.M., Pauken, K.E., Huang, A.C., et al. (2016). Tumor Interferon Signaling Regulates a Multigenic Resistance Program to Immune Checkpoint Blockade. Cell *167*, 1540–1554.e12.

64. Anfossi, N., André, P., Guia, S., Falk, C.S., Roetynck, S., Stewart, C.A., Breso, V., Frassati, C., Reviron, D., Middleton, D., et al. (2006). Human NK cell education by inhibitory receptors for MHC class I. Immunity *25*, 331–342.

65. Zhang, X., Feng, J., Chen, S., Yang, H., and Dong, Z. (2019). Synergized regulation of NK cell education by NKG2A and specific Ly49 family members. Nat. Commun. *10*, 5010.

66. Shreeve, N., Depierreux, D., Hawkes, D., Traherne, J.A., Sovio, U., Huhn, O., Jayaraman, J., Horowitz, A., Ghadially, H., Perry, J.R.B., et al. (2021). The CD94/NKG2A inhibitory receptor educates uterine NK cells to optimize pregnancy outcomes in humans and mice. Immunity *54*, 1231–1244.e4.

67. Rumpret, M., Drylewicz, J., Ackermans, L.J.E., Borghans, J.A.M., Medzhitov, R., and Meyaard, L. (2020). Functional categories of immune inhibitory receptors. Nat. Rev. Immunol. *20*, 771–780.

68. van der Burg, S.H., Visseren, M.J., Brandt, R.M., Kast, W.M., and Melief, C.J. (1996). Immunogenicity of peptides bound to MHC class I molecules depends on the MHC-peptide complex stability. J. Immunol. *156*, 3308–3314.

69. Kambayashi, T., Kraft-Leavy, J.R., Dauner, J.G., Sullivan, B.A., Laur, O., and Jensen, P.E. (2004). The nonclassical MHC class I molecule Qa-1 forms unstable peptide complexes. J. Immunol. *172*, 1661–1669.

70. Praest, P., Liaci, A.M., Förster, F., and Wiertz, E.J.H.J. (2019). New insights into the structure of the MHC class I peptide-loading complex and mechanisms of TAP inhibition by viral immune evasion proteins. Mol. Immunol. *113*, 103–114.

71. Hazini, A., Fisher, K., and Seymour, L. (2021). Deregulation of HLA-I in cancer and its central importance for immunotherapy. J. Immunother. cancer *9*, e002899.

72. Yewdell, J.W., Antón, L.C., and Bennink, J.R. (1996). Defective ribosomal products (DRiPs): a major source of antigenic peptides for MHC class I molecules? J. Immunol. *157*, 1823–1826.

73. He, W., Gea-Mallorquí, E., Colin-York, H., Fritzsche, M., Gillespie, G.M., Brackenridge, S., Borrow, P., and McMichael, A.J. (2023). Intracellular trafficking of HLA-E and its regulation. J. Exp. Med. *220*, e20221941.

74. Chapman, T.L., Heikeman, A.P., and Bjorkman, P.J. (1999). The inhibitory receptor LIR-1 uses a common binding interaction to recognize class I MHC molecules and the viral homolog UL18. Immunity *11*, 603–613.

75. Willcox, B.E., Thomas, L.M., and Bjorkman, P.J. (2003). Crystal structure of HLA-A2 bound to LIR-1, a host and viral major histocompatibility complex receptor. Nat. Immunol. *4*, 913–919.

76. Zeller, T., Lutz, S., Münnich, I.A., Windisch, R., Hilger, P., Herold, T., Tahiri, N., Banck, J.C., Weigert, O., Moosmann, A., et al. (2022). Dual checkpoint blockade of CD47 and LILRB1 enhances CD20 antibody-dependent phagocytosis of lymphoma cells by macrophages. Front. Immunol. *13*, 929339.

77. Zhao, J., Zhong, S., Niu, X., Jiang, J., Zhang, R., and Li, Q. (2019). The MHC class I-LILRB1 signalling axis as a promising target in cancer therapy. Scand. J. Immunol. *90*, e12804.

78. Sanson, K.R., Hanna, R.E., Hegde, M., Donovan, K.F., Strand, C., Sullender, M.E., Vaimberg, E.W., Goodale, A., Root, D.E., Piccioni, F., and Doench, J.G. (2018). Optimized libraries for CRISPR-Cas9 genetic screens with multiple modalities. Nat. Commun. *9*, 5416.

79. Doench, J.G., Fusi, N., Sullender, M., Hegde, M., Vaimberg, E.W., Donovan, K.F., Smith, I., Tothova, Z., Wilen, C., Orchard, R., et al. (2016). Optimized sgRNA design to maximize activity and minimize off-target effects of CRISPR-Cas9. Nat. Biotechnol. *34*, 184–191.

80. Stringer, B.W., Day, B.W., D'Souza, R.C.J., Jamieson, P.R., Ensbey, K.S., Bruce, Z.C., Lim, Y.C., Goasdoué, K., Offenhäuser, C., Akgül, S., et al. (2019). A reference collection of patient-derived cell line and xenograft models of proneural, classical and mesenchymal glioblastoma. Sci. Rep. *9*, 4902.

81. Dull, T., Zufferey, R., Kelly, M., Mandel, R.J., Nguyen, M., Trono, D., and Naldini, L. (1998). A third-generation lentivirus vector with a conditional packaging system. J. Virol. *72*, 8463–8471.

82. Stewart, S.A., Dykxhoorn, D.M., Palliser, D., Mizuno, H., Yu, E.Y., An, D.S., Sabatini, D.M., Chen, I.S.Y., Hahn, W.C., Sharp, P.A., et al. (2003). Lentivirus-delivered stable gene silencing by RNAi in primary cells. RNA *9*, 493–501.

83. Konermann, S., Brigham, M.D., Trevino, A.E., Joung, J., Abudayyeh, O.O., Barcena, C., Hsu, P.D., Habib, N., Gootenberg, J.S., Nishimasu, H., et al. (2015). Genome-scale transcriptional activation by an engineered CRISPR-Cas9 complex. Nature *517*, 583–588.

84. Hu, D., Ikizawa, K., Lu, L., Sanchirico, M.E., Shinohara, M.L., and Cantor, H. (2004). Analysis of regulatory CD8 T cells in Qa-1-deficient mice. Nat. Immunol. *5*, 516–523.

85. Van Kaer, L., Ashton-Rickardt, P.G., Ploegh, H.L., and Tonegawa, S. (1992). TAP1 mutant mice are deficient in antigen presentation, surface class I molecules, and CD4-8+ T cells. Cell *71*, 1205–1214.

86. Pérarnau, B., Saron, M.F., Reina San Martin, B., Bervas, N., Ong, H., Soloski, M.J., Smith, A.G., Ure, J.M., Gairin, J.E., and Lemonnier, F.A. (1999). Single H2Kb, H2Db and double H2KbDb knockout mice: peripheral CD8+ T cell repertoire and anti-lymphocytic choriomeningitis virus cytolytic responses. Eur. J. Immunol. *29*, 1243–1252.

87. Mähler Convenor, M., Mähler Convenor, M., Berard, M., Feinstein, R., Gallagher, A., Illgen-Wilcke, B., Pritchett-Corning, K., and Raspa, M. (2014). FELASA recommendations for the health monitoring of mouse, rat, hamster, guinea pig and rabbit colonies in breeding and experimental units. Lab. Anim. *48*, 178–192.

88. Hingorani, S.R., Wang, L., Multani, A.S., Combs, C., Deramaudt, T.B., Hruban, R.H., Rustgi, A.K., Chang, S., and Tuveson, D.A. (2005). Trp53R172H and KrasG12D cooperate to promote chromosomal instability and widely metastatic pancreatic ductal adenocarcinoma in mice. Cancer Cell *7*, 469–483.

89. Coin, I., Beyermann, M., and Bienert, M. (2007). Solid-phase peptide synthesis: from standard procedures to the synthesis of difficult sequences. Nat. Protoc. *2*, 3247–3256.

90. Salcedo, M., Bousso, P., Ljunggren, H.G., Kourilsky, P., and Abastado, J.P. (1998). The Qa-1b molecule binds to a large subpopulation of murine NK cells. Eur. J. Immunol. *28*, 4356–4361.

91. Achour, A., Michaëlsson, J., Harris, R.A., Ljunggren, H.-G., Kärre, K., Schneider, G., and Sandalova, T. (2006). Structural basis of the differential stability and receptor specificity of H-2Db in complex with murine versus human beta2-microglobulin. J. Mol. Biol. *356*, 382–396.

92. McCoy, A.J., Grosse-Kunstleve, R.W., Adams, P.D., Winn, M.D., Storoni, L.C., and Read, R.J. (2007). Phaser crystallographic software. J. Appl. Crystallogr. *40*, 658–674.

93. Liebschner, D., Afonine, P.V., Baker, M.L., Bunkóczi, G., Chen, V.B., Croll, T.I., Hintze, B., Hung, L.W., Jain, S., McCoy, A.J., et al. (2019). Macromolecular structure determination using X-rays, neutrons and electrons: recent developments in Phenix. Acta Crystallogr. D Struct. Biol. *75*, 861–877.

94. Emsley, P., Lohkamp, B., Scott, W.G., and Cowtan, K. (2010). Features and development of Coot. Acta Crystallogr. D Biol. Crystallogr. *66*, 486–501.

95. Chen, V.B., Arendall, W.B., 3rd, Headd, J.J., Keedy, D.A., Immormino, R.M., Kapral, G.J., Murray, L.W., Richardson, J.S., and Richardson, D.C. (2010). MolProbity: all-atom structure validation for macromolecular crystallography. Acta Crystallogr. D Biol. Crystallogr. *66*, 12–21.

96. Sanjana, N.E., Shalem, O., and Zhang, F. (2014). Improved vectors and genome-wide libraries for CRISPR screening. Nat. Methods *11*, 783–784.

97. Joung, J., Konermann, S., Gootenberg, J.S., Abudayyeh, O.O., Platt, R.J., Brigham, M.D., Sanjana, N.E., and Zhang, F. (2017). Genome-scale CRISPR-Cas9 knockout and transcriptional activation screening. Nat. Protoc. *12*, 828–863.

98. Spahn, P.N., Bath, T., Weiss, R.J., Kim, J., Esko, J.D., Lewis, N.E., and Harismendy, O. (2017). PinAPL-Py: A comprehensive web-application for the analysis of CRISPR/Cas9 screens. Sci. Rep. *7*, 15854.

99. Joosten, S.A., Sullivan, L.C., and Ottenhoff, T.H.M. (2016). Characteristics of HLA-E Restricted T-Cell Responses and Their Role in Infectious Diseases. J. Immunol. Res. *2016*, 2695396.

100. Baía, D., Pou, J., Jones, D., Mandelboim, O., Trowsdale, J., Muntasell, A., and López-Botet, M. (2016). Interaction of the LILRB1 inhibitory receptor with HLA class Ia dimers. Eur. J. Immunol. *46*, 1681–1690.

STAR★METHODS

KEY RESOURCES TABLE

REAGENT or RESOURCE	SOURCE	IDENTIFIER
Antibodies		
Anti-human CD11 b PE (clone D12)	BD Biosciences	Cat: 333142; RRID: AB_2868643
Anti-human CD11b PerCP-Cy5.5 (clone ICRF44)	BioLegend	Cat: 301328; RRID: AB_10933428
Anti-human CD11c BV510 (clone B-ly6)	BD Biosciences	Cat: 563026; RRID: AB_2737960
Anti-human CD123 SB436 (clone 6H6)	Thermo Fisher	Cat: 62-1239-42; RRID: AB_2662727
Anti-human CD14 PE-Cy7	BD Biosciences	Cat: 557742; RRID: AB_396848
Anti-human CD14 SparkBlue550 (clone 63D3)	BioLegend	Cat: 367148; RRID: AB_2832724
Anti-human CD141 BB515 (clone 1A4)	BD Biosciences	Cat: 565084; RRID: AB_2739058
Anti-human CD159a/NKG2A APC (clone Z199)	Beckman Coulter	Cat: A60797; RRID: AB_10643105
Anti-human CD19 Spark NIR685 (clone HIB19)	BioLegend	Cat: 302270; RRID: AB_2832581
Anti-human CD1c BUV661 (clone F10/213A3)	BD Biosciences	Cat: 750181; RRID: AB_2874384
Anti-human CD3 Pacific Orange (clone UCHT1)	Exbio	Cat: PO-514-T100; RRID: AB_10954113
Anti-human CD4 CF568 (clone C4/206)	Biotium	Cat: BNC680206-500; RRID: N/A
Anti-human CD45 PerCP (clone H130)	BioLegend	Cat: 304026; RRID: AB_893337
Anti-human CD47 (clone CC2C6)	Santa Cruz	Cat: sc-21786; RRID: AB_627087
Anti-human CD56 BV750 (clone 5.1H11)	BioLegend	Cat: 362556; RRID: AB_2801001
Anti-human CD8 BUV805 (clone SK1)	BD Biosciences	Cat: 612889; RRID: AB_2833078
Anti-human CD86 APC R700 (clone 2331)	BD Biosciences	Cat: 565149; RRID: AB_2739080
Anti-human HLA-A,B,C PE (clone W6/32)	BioLegend	Cat: 311406; RRID: AB_314875
Anti-human HLA-DR PE-Fire810 (clone L243)	BioLegend	Cat: 307683; RRID: AB_2904336
Anti-human HLA-DR V500 (clone G46-6)	BD Biosciences	Cat: 561224; RRID: AB_10563765
Anti-human HLA-E PE (clone 3D12)	BioLegend	Cat: 342604; RRID: AB_1659249
Anti-human IgG IRDye680RD	LI-COR	Cat: 926–68078; RRID: AB_10956144
Anti-human iNOS AF488 (clone 4E5)	Novus Biologicals	Cat: NBP2-22119; RRID: AB_2905500
Anti-human LILRB1 FITC (clone GHI/75)	Biolegend	Cat: 333729; RRID: AB_2888779
Anti-human PD-L1 BV650 (clone MIH1)	BD Biosciences	Cat: 563740; RRID: AB_2738398
Anti-mouse CD11b PE-Cyanine7 (clone M1/70)	Thermo Fisher	Cat: 25-0112-82; RRID: AB_469588
Anti-mouse CD11c APC-Cyanine7 (clone N418)	BioLegend	Cat: 117324; RRID: AB_830646
Anti-mouse CD159a/NKG2AB6 PE (clone 16A11)	BioLegend	Cat: 142803; RRID: AB_10959654
Anti-mouse CD16/CD32 Fc block (clone 2.4G2)	BD Biosciences	Cat: 553142; RRID: AB_394657
Anti-mouse CD19 FITC (clone 1D3)	Thermo Fisher	Cat: 11-0193-85; RRID: AB_657668
Anti-mouse CD19 PE (clone 1D3)	Thermo Fisher	Cat: 12-0193-82; RRID: AB_657659
Anti-mouse CD274 BV421 (clone MIH5)	BD Biosciences	Cat: 564716; RRID: AB_2738911
Anti-mouse CD3 eFluor 450 (clone 17A2)	Thermo Fisher	Cat: 48-0032-82; RRID: AB_1272193
Anti-mouse CD335/NKp46 BV421 (clone 29A.1.4)	BioLegend	Cat: 137612; RRID: AB_2563104
Anti-mouse CD3e FITC (clone 145-2C11)	Thermo Fisher	Cat: 11-0031-85; RRID: AB_464883
Anti-mouse CD4 BV605 (clone RM4-5	BioLegend	Cat: 100547; RRID: AB_11125962
Anti-mouse CD40 (clone FGK)	Produced in house	N/A
Anti-mouse CD45 AF700 (clone 30-F11)	BioLegend	Cat: 103128; RRID: AB_493715
Anti-mouse CD45.2 APC-eFluor780 (clone 104)	Thermo Fisher	Cat: 47-0454-82; RRID: AB_1272175
Anti-mouse CD62L BV421 (clone MEL-14)	BioLegend	Cat: 104436; RRID: AB_2562560
Anti-mouse CD86 FITC (clone GL-1)	Thermo Fisher	Cat: 11-0862-82; RRID: AB_465148
Anti-mouse CD86 PerCP-Cyanine5.5 (clone GL-1)	BioLegend	Cat: 105027; RRID: AB_893420
Anti-mouse CD8a AF700 (clone 53–6.7)	Thermo Fisher	Cat: 56-0081-82; RRID: AB_494005
Anti-mouse Egr2 PE (clone erongr2)	Thermo Fisher	Cat: 12-6691-82; RRID: AB_10717804

(*Continued on next page*)

Continued

REAGENT or RESOURCE	SOURCE	IDENTIFIER
Anti-mouse F4/80 PE (clone BM8)	BioLegend	Cat: 123110; RRID: AB_893486
Anti-mouse F4/80 PE-Cy7 (clone BM8)	BioLegend	Cat: 123114; RRID: AB_893478
Anti-mouse F4/80 PE-Cyanine5 (clone BM8)	BioLegend	Cat: 123112; RRID: AB_893482
Anti-mouse H-2K^{d} Pacific Blue	BioLegend	Cat: 116616; RRID: AB_1937242
Anti-mouse H-2L^{d}/H-2D^{b} PE (clone 28-14-8)	BioLegend	Cat: 114507; RRID: AB_313588
Anti-mouse I-A/I-E BV421 (clone M5/114.15.2)	BD Biosciences	Cat: 562564; RRID: AB_2716857
Anti-mouse IFN-γ APC (clone (XMG1.2)	BioLegend	Cat: 505810; RRID: AB_315404
Anti-mouse IgG AF647 (clone Poly4053)	BioLegend	Cat: 405322; RRID: AB_2563045
Anti-mouse iNOS AF488 (clone CXNFT)	Thermo Fisher	Cat: 53-5920-82; RRID: AB_2574423
Anti-mouse Ly-6C BV605 (Clone HK1.4)	BioLegend	Cat: 128036; RRID: AB_2562353
Anti-mouse Ly-6C BV785 (clone HK1.4)	BioLegend	Cat: 128041; RRID: AB_2565852
Anti-mouse Ly-6G BV785 (clone 1A8)	BioLegend	Cat: 127645; RRID: AB_2566317
Anti-mouse NK1-1 BV650 (clone PK136)	BD Biosciences	Cat: 564143; RRID: AB_2738617
Anti-mouse Qa-1^{b} biotin (clone 6A8.6F10.1.A6)	BD Biosciences	Cat: 559829; RRID: AB_397345
Anti-mouse Siglec-F BV711 (clone E50-2440)	BD Biosciences	Cat: 740764; RRID: AB_2740427
Anti-mouse Siglec-H BV650 (clone 440c)	BD Biosciences	Cat: 747672; RRID: AB_2744233
Anti-mouse TRP1 (clone TA99)	Santa Cruz	Cat: sc-58438; RRID: AB_793581
Anti-mouse/human CD44 BV786 (clone IM7)	BioLegend	Cat: 103059; RRID: AB_2571953
Human TruStain FcX	BioLegend	Cat: 422302; RRID: AB_2818986
Mouse IgG2A EXX1	Produced in house	N/A
Mouse IgG2A EXX1 AF647	Produced in house	N/A
Mouse IgG2A isotype control	Produced in house	N/A
Mouse IgG2A isotype control AF647	Produced in house	N/A
Bacterial and virus strains		
BL21 E. Coli	NEB	Cat: C25271
STBL3 bacteria	Thermo Fisher	Cat: C737303
Biological samples		
Human venous blood samples (for PBMC staining)	Healthy volunteers	N/A
Buffy coats (for macrophage cultures)	Sanquin	N/A
Chemicals, peptides, and recombinant proteins		
Aldara	3M pharma	N/A
Blasticidin	Thermo Fisher	Cat: A1113903
Bovine Serum Albumin	Sigma-Aldrich	Cat: A3912
Bromophenol blue	Merck	Cat: 108122
BsmBI	NEB	Cat: R0739L
Celltrace Far Red	Thermo Fisher	Cat: C34564
Cycloheximide	Sigma-Aldrich	Cat: C7698
Cytochalasin-D	Sigma-Aldrich	Cat: C8273
EDTA	Sigma-Aldrich	Cat: EDS
Ethylene glycol	Sigma-Aldrich	Cat: 102466
Geneticin	Gibco	Cat: 310131035
Glutathione (oxidized)	Sigma-Aldrich	Cat: G4376
Glutathione (reduced)	Sigma-Aldrich	Cat: G4251
Glycerol	Sigma-Aldrich	Cat: 49770
GolgiPlug protein transport inhibitor	BD Biosciences	Cat: 555029/51-2301KZ
Gp10020-39 peptide (AVGALKVPRNQDWLGVPRQL)	Produced in house	N/A
GSH	PanReach AppliChem	Cat: A2084

(*Continued on next page*)

Continued

REAGENT or RESOURCE	SOURCE	IDENTIFIER
GSSG	PanReach AppliChem	Cat: A2243
HPV16 E743-77 peptide (GQAEPDRAHYNIVTFCCKCDSTL RLCVQSTHVDIR)	Produced in house	N/A
iQ Sybr Green Supermix	BioRad	Cat: 1708887
Ketamine	Alfasan	ATCvet code: QN01AX03
L-arginine	PanReach AppliChem	Cat: A1700
L-glutamine	ATCC	Cat: 30-2214
Liberase TL	Roche	Cat: 05401020001
LILRB1-Fc	Sino Biological	Cat: 16014-H02H
Lipofectamine 3000	Thermo Fisher	Cat: L3000008
Lipopolysaccharides from E. Coli O26:B6	Sigma-Aldrich	Cat: L8274
Marizomib	MedChemExpress	Cat: HY-10985
MEM NEAA (100x)	Gibco	Cat: 11140-035
MgCl2	Sigma-Aldrich	Cat: M1028
Milk powder	Sigma-Aldrich	Cat: M7409
NaCl	VWR	Cat: 27810
NiCl2	Sigma-Aldrich	Cat: 33935
NP40	Merck Millipore	Cat: 492016
ODN-1826 (CpG)	Invivogen	Tlrl-1826-1
OVA peptide (SIINFEKL)	Produced in house	N/A
PEG4000	VWR	Cat: EM8.07490
Penicillin/streptomycin	ATCC	Cat: 30-2300
Penicillin-Streptomycin-Glutamine (100x)	Gibco	Cat: 10378016
PMSF	PanReach AppliChem	Cat: A0999
Polybrene	Merck Millipore	Cat: TR-1003-G
Polyethyleneimine	Polyscience Inc.	Cat: 23966-1
Protease inhibitors	Roche	Cat: 5056489001
Puromycin	Thermo Fisher	Cat: J672368EQ
Q001 peptide (AQAERTPEL)	Genscript	N/A
Q001/hβ2m/Qa-1^{b} tetramer APC	Produced in house	N/A
Qdm/hβ2m/Qa-1^{b} tetramer APC	Produced in house	N/A
Qdm peptide (AMAPRTLLL)	Genscript	N/A
Recombinant human GM-CSF	Immunotools	Cat: 11343127
Recombinant human IFN-γ	Peprotech	Cat: 300-02
Recombinant human IL-2 (Proleukin)	Clinigen	N/A
Recombinant murine GM-CSF	Peprotech	Cat: 315-03
Recombinant murine IFN-α	Miltenyi Biotech	Cat: 130-093-131
Recombinant murine IFN-γ	BioLegend	Cat: 575306
Recombinant murine IFN-λ	Tebu-bio	Cat: 250-33-A
Recombinant murine IL-4	Peprotech	Cat: 214-14
Recombinant murine M-CSF	Peprotech	Cat: 315-02
RLP peptide (RLPAKAPLL)	Produced in house	N/A
RMP peptide (RMPPLGHEL)	Produced in house	N/A
Sodium Acetate	Sigma-Aldrich	Cat: 241245
Sodium azide	In house pharmacy	N/A
Sodium pyruvate solution	Sigma-Aldrich	Cat: S8636
Streptavidin APC	Thermo Fisher	Cat: 17-4317-82

(*Continued on next page*)

Continued

REAGENT or RESOURCE	SOURCE	IDENTIFIER
Streptavidin APC	Cytekbio	Cat: 20-4317
Streptavidin IRDye 800CW	LI-COR	Cat: 926-32230
Streptavidin PE	Thermo Fisher	Cat: 12-4317-87
Streptavidin PE-CF594	BD Biosciences	Cat: 562318
Sulforhodamine 101/SR101	Sigma-Aldrich	Cat: S7635
T4 DNA ligase	Thermo Fisher	Cat: EL0011
Tilorone dihydrochloride	Sigma-Aldrich	Cat: 220957
Tris	PanReach AppliChem	Cat: A1379
Tris-HCl	Combi Blocks	Cat: OR-5119
Tween 20	Sigma-Aldrich	Cat: P1379
Urea	Thermo Fisher	Cat: J75826.A7
VLR peptide (VLRPGGHFL)	Produced in house	N/A
VMAPJTLVL peptide	Produced in house	N/A
VML peptide (VMAPRTLIL)	Produced in house	N/A
Xylazine	Dechra	ATCvet code: QN05CM92
β-mercaptoethanol	Millipore-Sigma	Cat: 63689
Critical commercial assays		
BirA Biotin Ligase Kit	Avidity	N/A
Cell trace CFSE cell proliferation kit	Thermo Fisher	Cat: C34554
Click-it sDIBO alkyne kit for antibody labeling (Alexa Fluor 647)	Thermo Fisher	Cat: C20029
FoxP3/Transcription Factor Staining Buffer Set	Thermo Fisher	Cat: 00-5523-00
High-Capacity RNA-to-cDNA Kit	Thermo Fisher	Cat: 4387406
Isolate II genomic DNA kit	GC Biotech	Cat: BIO-52067
Magnisort Mouse NK Cell Enrichment Kit	Thermo Fisher	Cat: 8804-6828-74
NebBuilder Hi-Fi Assembly	New England Biolabs	Cat: E5520
Nucleospin Plasmid Transfection Grade Kit	Macherey-Nagel	Cat: 740.490.250
Nucleospin RNA Plus Kit	Macherey-Nagel	Cat: 740984.50
SiteClick antibody azido modification kit	Thermo Fisher	Cat: S20026
Untouched Pan Monocyte Isolation Kit	Miltenyi Biotech	Cat: 130-096-537
Zombie Aqua Fixable Viability Kit	BioLegend	Cat: 423102
Zombie NIR Fixable Viability Kit	BioLegend	Cat: 423106
Zombie UV Fixable Viability Kit	BioLegend	Cat: 423107
Deposited data		
Crystal structure Q001/Qa-1[b]	Protein database	PDB ID: 8P43
Experimental models: Cell lines		
2B4-LILRB1 reporter cells	Dr. M. López Botet	N/A
A20	Dr. P. André	RRID:CVCL_1940
A20-eGFP-Neo/Fluc-Puro	Imanis Life Science	Cat: CL152
B16F10	ATCC	Cat: CRL6475, RRID:CVCL_0159
Expi293F	Thermo Fisher Scientific	Cat: A14527, RRID:CVCL_D615
FGK-45	Dr. A. Rolink	N/A
HEK293T	ATCC	RRID:CVCL_0063
J774	ATCC	Cat: 85011428, RRID:CVCL_4692
K562	Yvonne Zoet	RRID:CVCL_0004
K562.HLA-E	Dr. M. Lampen	N/A
KPC3	Dr. F. Balkwill	RRID:CVCL_A9ZK
Phoenix ampho	Dr. M. Heemskerk	RRID:CVCL_H716

(*Continued on next page*)

Continued

REAGENT or RESOURCE	SOURCE	IDENTIFIER
Raji	Dr. M. Heemskerk	RRID:CVCL_0511
RAW264.7	Dr. F. Ossendorp	RRID:CVCL_0493
RMA	Dr. K Kärre	RRID:CVCL_J385
TC1	Dr. T.C. Wu	RRID:CVCL_4699
Experimental models: Organisms/strains		
BALB/cAnNCrl	Charles River, USA	Cat: 028
C57BL/6J	Charles River, The Netherlands	Cat: 632
H2-D^b KO BL/6, B6.129P2-H2-Db^{tm1} N12	Francois Lemonnier	N/A
NKG2A KO BL/6, B6.KLRC1^{em2lumc}	This manuscript	MGI: 6473464
Qa-1^b KO BL/6, B6.129S6-H2-$T23^{tm1Cant}$/J	Jackson Laboratories	Cat: 007907
Tap1 KO BL/6, B6.129S2-$Tap1^{tm1Arp}$/J	Jackson Laboratories	Cat: 002944
TCR transgenic $gp100_{25\text{-}33}$/H2-D^b Pmel BL/6	Dr. N.P. Restifo	N/A
Oligonucleotides		
Table S5	This manuscript	N/A
Recombinant DNA		
CDS Codon-optimized extracellular Qa-1^b for tetramers (*H2-T23*)	Genscript	N/A
CDS Codon-optimized human CD94 (*Klrd1*)	Twist Bioscience	N/A
CDS Codon-optimized human NKG2A (*Klrc1*)	Twist Bioscience	N/A
CDS Codon-optimized human β2m for tetramers (*β2m*)	Genscript	N/A
CDS Codon-optimized LILRB1 (*Lilrb1*)	Integrated DNA Technologies	N/A
CDS Codon-optimized LILRB2 (*Lilrb2*)	Integrated DNA Technologies	N/A
CDS Codon-optimized Qa-1^b heavy chain for cell lines (*H2-T23*)	Twist Bioscience	N/A
Genome-wide Calabrase activation library (sublibrary A + B)	Sanson et al.[78]	Addgene cat: 1000000111
Genome-wide mouse CRISPR Brie knockout library	Doench et al.[79]	Addgene cat: 73632
Plasmid pFUSE-mouse (m)IgG2A-Fc2	Invivogen	Cat: pfuse-mg2afc2
Plasmid LentiCRISPRv2 puro	Stringer et al.[80]	Addgene Cat: 98290
Plasmid Pax2	Dr. D. Trono	Addgene Cat: 12260
Plasmid pMD2.G	Dr. D. Trono	Addgene Cat: 12259
Plasmid pMX	Dr. T. Schumacher	N/A
Plasmid pCDH-CMV-MCS-EF1-Puro	System Biosciences	Cat: CD510B-1
Plasmid pET-30a_Qa-1b	Dr. K. Söderström	Addgene Cat: 211369
Plasmid pET-3a_mβ2m	Dr. J. Michaelsson	Addgene Cat: 211368
Plasmid pET-21a(+)	Millipore-Sigma	Cat: 69740
Plasmid pMDLg/PRRE	Dull et al.[81]	Addgene Cat: 12251
Plasmid pRSV-Rev	Dull et al.[81]	Addgene Cat: 12253
Plasmid pCMV-VSV-G	Stewart et al.[82]	Addgene Cat: 8454
Plasmid dCAS-VP64_Blast	Konermann et al.[83]	Addgene Cat: 61425
Plasmid pXPR_502	Sanson et al.[78]	Addgene Cat: 96923
Plasmid pLenti_P2A_Puro	This manuscript	Addgene Cat: 211364
Software and algorithms		
BioRender	BioRender	RRID: SCR_018361; http://biorender.com/

(*Continued on next page*)

Continued

REAGENT or RESOURCE	SOURCE	IDENTIFIER
COOT V.0.9	N/A	RRID: SCR_014222; https://www2.mrc-lmb.cam.ac.uk/personal/pemsley/coot/docs/coot-faq.html#Citing
FlowJo V.10	Treestar	RRID: SCR_008520; https://www.flowjo.com/solutions/flowjo
GraphPad Prism V.9	GraphPad	RRID: SCR_002798; http://www.graphpad.com/
MolProbity V.1.19.1–4122	Phenix	RRID: SCR_014226; https://phenix-online.org/
OMIQ	Omiq Inc.	https://www.omiq.ai
PHASER V.1.19.1–4122	Phenix	https://phenix-online.org/
Phenix Refine V.1.19.1–4122	Phenix	RRID: SCR_014224; https://phenix-online.org/
PinAPL-PY	University of San Diego, California	http://pinapl-py.ucsd.edu/
Other		
DPBS	Gibco	Cat: 14040133
FBS	Cytivalifescience	Cat: SH30088.03HI
FCS	Bodinco	Cat: 5010
Ficoll	In house pharmacy	N/A
Hiload 16/60 Superdex 75	GE-Healthcare	Cat: 17-1068-01
Hiload 26/600 Superdex 200	Cytivalifescience	Cat: 28989336
Hiload 26/600 Superdex 75	Cytivalifescience	Cat: 28989334
Iscove's Modified Dulbecco's Medium (IMDM)	Gibco	Cat: 12440
Lysis buffer (red blood cells)	In house pharmacy	N/A
Matrigel	Millipore-Sigma	Cat: CLS354248
Nuclease-free water	In house pharmacy	N/A
Nylon wool	Baseclear	Cat: MKN-50
PBS	Fresenius Kabi	N/A
Protein A resin	Genscript	Cat: L00210
Protein G Sepharose 4 FF	Sigma-Aldrich	Cat: GE17-0618-01
RPMI-1640	Cytivalifescience	Cat: SH30605

RESOURCE AVAILABILITY

Lead contact

Further information and requests for resources or reagents should be directed to and will be fulfilled up to reasonable request by the lead contact, Thorbald van Hall (t.van_hall@lumc.nl).

Materials availability

The pLenti_P2A_Puro plasmid generated in this study has been deposited to Addgene (Cat: 211364).

Information about the NKG2A KO mouse (*Klrc1*^{em2Lumc}) generated in this study has been deposited to Jax (MGI:6473464). Mice will be provided upon request directed to the lead contact.

Data and code availability

- The crystal structure of Q001/Qa-1^{b} that was generated in this study has been deposited to the protein database (PDB: 8P43).
- This paper does not report original code.
- Any additional information required to reanalyze the data reported in this paper is available from the lead contact upon request.

EXPERIMENTAL MODEL AND STUDY PARTICIPANT DETAILS

Mice

C57BL/6J and BALB/c mice were purchased from Charles River, the Netherlands or the United States, respectively. Qa-1^{b}-deficient[84] and Tap1-deficient[85] C57BL/6 mice were initially obtained from Jackson Laboratories (B6.129S6-H2-T23^{tm1Cant}/J, stock number 007907 and B6.129S2-Tap1^{tm1Arp}/J, stock number 002944, respectively) and bred at the Leiden University Medical Center (LUMC). H-2D^{b}-deficient C57BL/6 mice[86] (B6.129P2-H2-*Db*^{tm1} N12, Taconic stock number 4217) were kindly provided by Dr. F. Lemonnier of the Institut Pasteur in Paris, France. T cell receptor (TCR) transgenic mice containing gp100$_{25\text{-}33}$/H-2D^{b} specific receptors (designated as pmel) were kindly provided by Dr. N.P. Restifo (Center for Cancer Research, National Cancer Institute, NIH, Bethesda, MD), and were bred at the LUMC unto a congenic CD45.1 background. NKG2A-deficient C57BL/6 mice (Klrc1^{em2LUMC}, MGI 6473464) were generated at the LUMC by electroporating C57BL/6J zygotes with CRISPR/Cas9 RNP complexes targeting *Klrc1* intron 2 (sgRNA ATCTCAGTAAAGAATCTCCA) and intron 4 (sgRNA CTACAGGTTGAAAACTGCTG) followed by transfer to pseudo-pregnant females. From the resulting animals a founder was selected carrying a 1427 nt deletion in *Klrc1* (GRCm39 6:129653615-129655041) encompassing exon 3 and 4 of the gene. The founder animal was further bred to C57BL6/J to generate the mouse line. Genomic DNA of the pups obtained via ear puncture was screened by Transnetyx using the following probe sequences: *Klrc1* KO, forward primer 5′ GTGGAATGGTTGTTATGATATTCAGAATATTATGACTATCA 3′, reporter 5′ CAATGATTCCCT AACTTAAAC 3′, reverse primer 5′ GTCATTCTACTCCACTAAGGGTTGTAATCTACA 3’; *Klrc1* WT forward primer 5′ CAGAATATTATG ACTATCAGAGGAATTGTATAAATG 3′, reporter 5′ AGCCTTGGAGATTCTTTAC 3′, reverse primer 5′ CTATGACAAAACCACTTTCC AAACAG 3’. Additionally, blood of pups lacking the *Klrc1* gene was screened for the absence of NKG2A using flow cytometry.

Mouse experiments were performed at the animal facility of the LUMC and were approved by the Dutch animal ethics committee (CCD) and the local Animal Welfare Body on the permit numbers AVD116002015271 and AVD11600202010004. The survival study with EXX1 treatment was performed at the animal facility of the University of Texas, Arlington (UTA), United States of America under the institutional animal care and use committee (IACUC). The health status of the animals was monitored over time and all animals were tested negative for agents listed in the FELASA (Federation of European Laboratory Animal Science Associations) guidelines for specific-pathogen free (SPF) mouse colonies.[87] Mice were allowed to acclimate to the housing facility for one week prior to starting experiments. Experiments were performed in accordance with the Dutch Act on Animal Experimentation and EU Directive 2010/63/EU (’On the protection of animals used for scientific purposes’).

Human subjects

Venous blood samples were drawn from healthy volunteers after giving informed consent. Usage of blood samples from healthy volunteers was approved by the departmental ethical committee of the LUMC. Buffy coats were obtained from the Sanquin blood bank, Amsterdam. Usage of buffy coats has been approved by the ethical committee (EAR) of Sanquin. Blood samples were diluted with PBS, added on top of a 15 mL Ficoll layer in 50 mL tubes and then centrifuged for 15 min at 2200 rpm at the lowest brake setting. The interphase was collected and washed twice with PBS to remove the remaining Ficoll, resulting in peripheral mononuclear cells (PBMCs).

Cell lines

The B16F10 melanoma cell line (RRID:CVCL_0159) was purchased from the American Type Culture Collection (ATCC). The TC1 tumor cell line (RRID:CVCL_4699) expresses the HPV16-derived E6 and E7 oncogenes and activated Ras oncogene and was kindly gifted by T.C. Wu (John Hopkins University, Baltimore, USA). The KPC3 murine pancreatic carcinoma (RRID:CVCL_A9ZK) with mutant *K-ras* and *p53* is derived from a primary tumor in a genetically engineered C57BL/6 mouse model and was provided by Dr. F. Balkwill.[88] RMA (RRID:CVCL_J385) is a Raucher MuLV-induced T cell lymphoma RBL-5 cell line and was originally obtained from Dr. K Kärre (Karolinska Institute, Stockholm, Sweden). All of the abovementioned cell lines were derived from C57BL/6 mice. The BALB/c macrophage cell line RAW264.7 (RRID:CVCL_0493) was kindly provided by Dr. F. Ossendorp (LUMC, Leiden, the Netherlands). The BALB/c A20 B cell lymphoma cell line (RRID:CVCL_1940) was obtained from Dr. P. André (Innate Pharma, Marseille, France). A20-eGFP-Neo/Fluc-Puro was purchased from Imanis Life Science. The BALB/c J774 monocyte/macrophage cell line (RRID:CVCL_4692) was purchased from the ATCC. Expi293F cells (RRID:CVCL_D615) were purchased from Thermo Fisher Scientific. The FGK-45 hybridoma was kindly provided by Dr. A. Rolink. The K562 lymphoblast cell line (RRID:CVCL_0004) was isolated from the bone marrow of a patient with chronic myelogenous leukemia and was obtained from Yvonne Zoet (LUMC, Leiden, the Netherlands). The K562.HLA-E cell line was a kind gift of Dr. M. Lampen. Phoenix-Ampho cells (RRID:CVCL_H716) and Raji cells (RRID:CVCL_0511) were kindly provided by Dr. M. Heemskerk. 2B4-LILRB1 reporter cells were kindly provided by Dr. M. López Botet. Finally, HEK293T cells (RRID:CVCL_0063) were purchased from the ATCC.

Unless indicated otherwise, all cell lines were cultured in Iscove’s modified Dulbecco’s medium (IMDM, Invitrogen) supplemented with 8% FCS (Greiner), 2% penicillin/streptomycin (Gibco) and 2mM glutamine (Gibco) at 37°C and 5% CO_2. Additionally, TC1 cells were supplemented with 400 μg/mL neomycin (G418, Life Technologies), 1x non-essential amino acids (Gibco) and 1mM sodium pyruvate (Life Technologies). A20-eGFP-Neo/Fluc-Puro cells were cultured in RPMI-1640 medium (Cytivalifescience), which was supplemented with 10% FBS (Cytivalifescience), 2% glutamine (ATCC) and penicillin/streptomycin (ATCC), 50 μM β-mercaptoethanol (Millipore-Sigma) and 1 mg/mL neomycin (Gibco) and 1 μg/mL puromycin (Thermo Fisher). The B16F10, TC1, KPC3, RMA and

A20 cell lines were authenticated by IDEXX bioanalytics using short tandem repeat markers and all cell lines were frequently tested for mycoplasma. For *in vivo* studies, cells were tested for known mouse pathogens using MAP tests.

METHOD DETAILS

Generation of peptides, proteins and antibodies

AMAPRTLLL (Qdm), AQAERTPEL (Q001) and SIINFEKL (OVA) peptides were produced by Genscript Biotech (Piscataway, New Jersey, USA). VMAPRTLIL (VML), VLRPGGHFL (VLR), RMPPLGHEL, RLPAKAPLL and peptides for immunization of mice ($gp100_{20-39}$, or HPV16 $E7_{43-77}$) were produced in house using solid phase peptide synthesis.[89]

The EXX1 and isotype control (targeting human CD3) antibody were produced as mouse IgG2a chimeric molecules (ATUM, Newark, California) by transfection of Expi293F cells (Thermo Fisher) with the pFUSE-mouse (m)IgG2A-Fc2 vector (Invivogen) containing the VHH region of EXX1 or anti-hCD3e.[34] Five days post transfection, supernatant was harvested and antibodies were purified using protein A resin (Genscript) according to the manufacturer's instructions. Antibody purity was confirmed using SDS-PAGE and analytical-grade Superdex 200 columns. For flow cytometry purposes, the EXX1 and isotype control antibodies were conjugated using the SiteClick antibody azido modification kit (ThermoFisher) and subsequently labeled with Alexa Fluor 647 due using the SiteClick sDIBO alkyne kit for antibody labeling (ThermoFisher), both according to the manufacturer's protocol.

Agonistic anti-mouse CD40 antibodies (clone FGK) were produced using the FGK-45 hybridoma (kindly provided by Dr. A. Rolink) and purified using protein G beads (Sigma-Aldrich) according to the manufacturer's protocol.[50] Qdm/Qa-1^b and Q001/Qa-1^b tetramers were generated by cloning the extracellular domain of mouse Qa-1^b containing a C terminus BirA peptide sequence for biotinylation and human β_2-microglobulin (β_2M) genes in pET21(+) vectors and used these to transform into BL21 *E. coli* (DE3) (NEB). Proteins were produced, purified from inclusion bodies, and used in refolding reactions with synthesized peptides (Genscript) to produce Qa-1^b/peptide complex.[90] The Qa-1^b/peptide mixture was concentrated, and the correctly folded complex was isolated from impurities using size exclusion chromatography (SEC) on a Superdex 75 (S75). A portion of the purified refolded complex, designated as active monomer, was biotinylated using the BirA biotin ligase enzyme (Avidity) and purified a second time on the S75 column. Purified material (biotinylated) was analyzed on a Sciex X500B QTOF mass spectrometer to detect Qa-1^b heavy chain, β_2M, peptide (indicating peptide loading) and the percentage of material that was biotinylated (for biotin-labeled molecules). Biotin-labeled monomer was then used to generate tetramer complexes by addition of allophycocyanin streptavidin (Cytekbio). Tetramer complexes were purified on a Superdex 200 (S200) sizing column and run on an NGC medium-pressure fast chromatography system (Bio-Rad). Purified tetramers were used in tetramer staining assays. All mass spectrometry work was performed at the Proteomics Core Lab at the University of Texas Southwestern Medical Center.

HLA-E*01:03 tetramers were produced using UV-mediated peptide exchange. Recombinant HLA-E*01:03 heavy chains with a C-terminal BirA recognition site and human β2-microglobulin (β2m) were produced in E. coli. HLA monomers were made by folding 2.5 mg of heavy chain with 1.2 mg of β2m and 3 mg UV-sensitive peptide (VMAPJTLVL, produced in house, where J is 2-nitrophenylamino acid) in 50 mL folding buffer (400 mM L-Arginine (PanReach Applichem), 0.5 mM oxidized glutathione(Sigma Aldrich), 5 mM reduced glutathione (Sigma Aldrich), 2 mM EDTA (Sigma Aldrich), 100 mM Tris.HCl (Combi Blocks) pH 8, glycerol 5% ((Sigma Aldrich) and half a tablet of protease inhibitor cocktail (Roche)). Monomers were biotinylated using the BirA enzyme and purified by gel filtration on a Hiload 16/60 Superdex 75 prep grade (GE-Healthcare) and stored in PBS 16% glycerol (Sigma Aldrich) at −80°C. UV-sensitive MHC-E monomer (0,5μm) was incubated in the presence of 100 μM exchange peptide (VMAPRTLIL, RMPPLGHEL, RLPAKAPLL and VLRPGGHFL (all produced in house)) in 25 μL exchange buffer (20 mM Tris (PanReach Applichem), 150 mM NaCl (Sigma Aldrich)). Exposure to UV light >350 nm for 60 min in a polypropylene U-bottom 96-well plate (Greiner Bio-One) at 4°C triggered the UV-mediated peptide exchange reaction. The biotinylated monomers were conjugated to PE-streptavidin (Thermo Fisher), resulting in PE-labeled HLA-E tetramers.

Generation, crystallization and analysis of the Q001/Qa-1^b peptide complex

BL21 (DE3) E. Coli expression cells were transfected separately with a pET-30a expression vector containing the CDS for Qa-1^b heavy chain (kindly provided by Dr. Kalle Söderström) and a pET-3a expression vector containing the mouse β2m (kindly provided by Dr. Jakob Michaelsson[91]). Inclusion bodies were isolated and solubilized in unfolding buffer (8 M urea (Thermo Scientific), 100 mM Tris (PanReach Applichem) and 2 mM EDTA (PanReach Applichem)). For refolding of Qa-1^b with mβ2m and Q001 peptide, 10 mg peptide was resuspended in 5 mL refolding buffer (100 mM Tris, 400 mM L-arginine (PanReach AppliChem), 2 mM EDTA, 0.5 mM glutathione disulfate (GSSG, PanReach AppliChem), 5 mM glutathione (GSH, PanReach AppliChem) and 0.5 mM PMSF (PanReach Applichem) and added dropwise to 1 L buffer on a magnetic stirrer at 4°C. Pre-heated (5 min at 42°C) β2m (24 mg) was added to the refolding mixture after peptide injection. After 30 min Qa-1^b (10 mg) was injected three consecutive times with 3 h interval between each addition. After 24 h, aggregates were removed using a rapid-filtermax 0.22 μm vacuum filter (Thermo Scientific) and the refolded protein complex was first concentrated using a peristaltic pump (Vivaflow 200, 30K MWCO, Sartorius) and then using centrifugal filtration with a 30K filter (Vivaspin). Finally, the refolded complexes were purified using size exclusion chromatography on an Äkta Purifier (GE Healthcare), followed by validation using SDS-PAGE.

Pure Q001/Qa-1^b complex was concentrated to 10 mg/mL by centrifugal filtration (Vivaspin, 30k MWCO) and then diluted to 4 mg/mL in size exclusion buffer (filtered 10 mM Tris, 150 mM NaCl (VWR), pH 8.0). Crystals grew in 10 days with a reservoir solution of 8%

PEG4000 (VWR), 0.1M sodium acetate (pH 5.7, Sigma-Aldrich) and 10 mM $NiCl_2$ (Sigma-Aldrich) with hanging drop vapor diffusion at 20°C. Prior harvesting, 20% ethylene glycol (Sigma-Aldrich) was added to the hanging drop as a cryoprotectant. Then, crystals were flash frozen in liquid nitrogen and stored in an UniPuck (Molecular Dimensions).

Diffraction data were collected at the BioMax MaxIV facility (Lund, Sweden). Phase information was obtained by molecular replacement in PHASER (Phenix - version 1.19.1–4122[92]) using the published structure of Qa-1b with Qdm peptide (PDB accession number: 3VJ6) as a ref. [16]. The electron density map was refined using the atomic positions of the Qdm reference peptide in Phenix Refine (Phenix - version 1.19.1–4122[93]) until reaching an Rwork of 19.3% and Rfree of 24.9%. From the refined electron density map, atomic positions of the 001 peptide were derived and modeled in COOT (Version 0.9).[94] Validation of the obtained structure was performed in MolProbity (Phenix - version 1.19.1–4122[92,95]), showing 96% Ramachandran favored residues and no outliers (0.79%).

Stimulation of cell lines for flow cytometry experiments

Unless indicated otherwise, cell lines were stimulated for two days as follows: A20, 30 IU/mL IFN-γ (BioLegend) and 10,000 IU/mL IFN-α (Miltenyi Biotech); B16F10, 30 IU/mL IFN-γ; RAW264.7, 5 IU/mL IFN-γ; RMA 30 IU/mL IFN-γ.

Flow cytometry

Single cell suspensions of cell lines, mouse tissues or tumors were generated. Cell suspensions of TC1 tumors were prepared by physical fragmentation, followed by 10 min incubation with 2.5 mg/mL liberase (Roche) at 37°C in a humidified atmosphere containing 5% CO_2. Then, cell suspensions from TC1 tumors, or whole B16F10 tumors were minced through a 70 μm cell strainer and plated in FACS plates. Mouse Fc-receptors were blocked by Rat Anti-Mouse CD16/CD32 (Clone 2.4G2, BD) for 15 min at 4°C in PBS. Human Fc receptors were blocked by incubation with TruStain FcX (BioLegend) for 10 min at 4°C. Viability was assessed with the LIVE/DEAD Fixable Aqua Dead Cell Stain Kit (BioLegend), Zombie NIR fixable viability kit (BioLegend), or Zombie UV fixable viability kit (BioLegend) in PBS before surface staining. Tetramers of APC-conjugated Qdm/Qa-1^b, Q001/Qa-1^b, or PE-conjugated HLA-E*01:03/VML, or HLA-E*01:03/VLR were stained for 30 min at RT in FACS buffer (PBS supplemented with 0.5% BSA (Sigma-Aldrich) + 0.002% sodium azide (in house pharmacy)). Then, other surface markers were stained in FACS buffer for 20 min at 4°C. If intracellular markers were present in the staining panel, cells were fixed and permeabilized using the FoxP3/Transcription Factor Staining Buffer Set (eBioscience) according to manufacturer's protocol. Finally, cells were resuspended in FACS buffer and measured on a Fortessa cytometer (BD bioscience), or Aurora 5L spectral flow cytometer (Cytek) and analyzed with FlowJo software v10.8.1 (Treestar) or OMIQ software, respectively. An overview of all the antibodies used for flow cytometry is shown in the resources table.

Generation of knockout and overexpression cells

Knockout cell lines were generated using CRISPR/Cas9 vector systems generated by the Zhang lab.[96] Mouse cell lines B16F10, RMA, A20 and RAW264.7 were targeted with sgRNAs for Qa-1^b (5′ GGCTATGTCATTCGCGGTCC 3′), Erap1 (5′ AGGGCAGGTT CATCAAAGCA 3′), or Tap1 (5′ CCTAGGACTAGGGGTCCGCG 3′) (Sigma Aldrich). Raji cells were targeted with sgRNAs for MHC class I (5′ CGGCTACTACAACCAGAGCG 3′), or HLA-E (5′ CGGGCCGGGACACGGAAGTG 3′). sgRNAs were designed using Benchling and Crispor online software with additional base pairs on each oligo to allow ligation into the target vector: 5′ CACCG(sgRNA1) 3′ and 3′ C(complementary sequence to sgRNA1)CAAA 5'. Complementary sgRNAs were annealed and ligated using T4 DNA ligase (Thermo Scientific) into a BsmBI-digested (NEB) lentiCRISPRv2 puro vector (Addgene). The plasmid constructs were propagated in STBL3 bacteria (Invitrogen) and isolated using nucleospin plasmid transfection grade kits (Macherey-Nagel) according to the manufacturers' protocol. HEK 293T cells were transfected with the lentiCRISPRv2 knockout constructs and accessory Pax2 and pMD2.G plasmids (both kindly gifted by Dr. Didier Trono) using lipofectamine 2000 (Invitrogen) according to the manufacturers' protocol. Then, supernatant of the HEK 293T cells containing the lentivirus was used to transduce the target cell lines. After puromycin antibiotic (Thermo Fisher) selection, the cell lines were cell sorted using flow cytometry based on Qa-1^b expression (6A8 antibody) for the Qa-1^b KO cells, based on Qdm/Qa-1^b expression (EXX1 antibody) for the Erap1 KO cells, or based on H-$2D^b$ expression for the Tap1 KO cells.

K562.NKG2A/CD94 was generated by transduction of K562 cells with retroviral particles from amphotropic phoenix cells transfected with two separate pMX plasmids (obtained from Dr. T. Schumacher) encoding human NKG2A and CD94. Transduced cells were sorted using flow cytometry based on surface NKG2A and CD94 expression. K562.Qa-1^b cells were generated by transduction of K562 cells with lentiviral particles from HEK293T cells, which were transfected with a pCDH-CMV-MCS-EF1-Puro plasmid (System Biosciences) encoding Qa-1^b and accessory Pax2 and pMD2.G plasmids similar to the knockout cells. Transduced cells were sorted using flow cytometry based on surface Qa-1^b expression (6A8 antibody). To generate K562.LILRB1 and K562.LILRB2 cells using activating gRNAs, K562 cells were first transduced with lentiviral particles from HEK293T cells, which were transfected with the Lenti dCas-VP64 plasmid (kindly provided by Dr. F. Zhang) and selected using blasticidin (Thermo Fisher). Next, these cells were transduced with lentiviral particles from HEK293T cells, which were transfected with the pXR_502 plasmid (Addgene) containing a gRNA for LILRB1 (5′ AAGACTCAGAGATTTGTTCC 3′) or LILRB2 (5′ CTCAGAGGTTTCTTCCCGGG 3′). To generate LILRB1-expressing cells using cDNA, K562 or J774 cells were transduced with lentiviral particles from HEK293T cells, which were transfected with a pLenti cloning vector plasmid containing cDNA for LILRB1 or LILRB2. The pLenti cloning vector was generated by amplifying the lentiCRISPR v2 backbone to exclude the Cas9 and gRNA elements using the Lenti 0 FW (5′ ATCCCGGCCCAAAC

AAGATAGCAACAAACTTCTCTCTGCTGAAACAAG 3′) and Lenti 0 RV (5′ CCAAACTGGATCTCTGCTGTCCC 3′) primers. Then, the EF-1a promotor was amplified separately using the Lenti EF-1a FW (5′ ACAGCAGAGATCCAGTTTGGCGCTAGCTAGGTCTTG AAAGGAGTG 3′) and Lenti EF-1a RV (5′ ACCGGTGGTACCTTAATTAACGGTCCTGTGTTCTGGCG 3′) primers. Finally, these two fragments were combined together with the MCS T2A oligo (5′ TTAATTAAGGTACCACCGGTAGAATTCAGATATCACT CGAGAGGATCCGGCGAGGGCAGGGGAAGTCTACTAACATGCGGGGACGTGGAGGAAAATCCCGGCCCAAACAAGATA 3′) using NebBuilder Hi-Fi Assembly (New England Biolabs). The cDNA was cloned into the expression vector using Gibson assembly with the following primers: LILRB1 FW 5′ ACACAGGACCGTTAATTAAGGTACCCACCATGACCCCCATCCTCACG 3′, LILRB1 RV 5′ GGATCCTCTCGAGTGATATCTGAATTCGTGGATGGCCAGAGTGGCGT 3′, LILRB2 FW 5′ ACACAGGACCGTTAATTAAGGTACCCA CCATGCACCGAGGGCTCATC 3′, LILRB2 RV 5′ GGATCCTCTCGAGTGATATCTGAATTCGTGGATGGCCAGGGTGGCG 3’.

Generation and phagocytosis of murine *ex vivo* macrophages and DCs

Murine bone marrow-derived macrophages (BMDMs) and -dendritic cells (BMDCs) were obtained by harvesting the femur and tibia of naive mice, which were flushed with standard IMDM cell culture medium (8% FCS and pen/strep). Erythrocytes were lysed with lysis buffer (in house pharmacy) and bone marrow cells were filtered through a 70 μm cell strainer (BD Biosciences). For BMDMs, the dissociated cells were plated into tissue-culture treated petri dishes (Greiner) and incubated for 4 h at 37°C and 5% CO_2 to eliminate tissue-resident macrophages, which attach to the culture dish. The non-adherent cells were cultured in fresh plates using standard IMDM supplemented with 20 ng/mL macrophage colony stimulating factor (M-CSF, Peprotech) in tissue-culture treated petri dishes for eight days. For BMDCs, the dissociated cells were plated in non-coated petri dishes (Greiner) with 20 ng/mL granulocyte-macrophage colony stimulating factor (GM-CSF, Peprotech) and 2 ng/mL IL-4 (Peprotech). After seven days of culture, BMDMs were stimulated for one day with 100 ng/mL LPS (Sigma-Aldrich) + 20 IU/mL IFN-γ (M1), with 20 ng/mL IL-4 (M2), or culture medium (M0). Similarly, BMDCs were stimulated for one day with 100 ng/mL LPS (mature DC) or culture medium (immature DC).

Alternatively, splenic-derived macrophages were generated similar to BMDMs with the only exception that splenocytes were used as source of the macrophages instead of bone marrow cells and that there was no additional adhesion step to get rid of the tissue-resident macrophages.

Then, cells were subjected to flow cytometry and phagocytosis assays. For phagocytosis studies, target cells (B16F10.Qa-1$^+$ and B16.Qa-1$^-$ pre-stimulated for two days with 30 IU/mL IFN-γ) were irradiated with 6000 Rad and labeled with 5 μM CFSE (Thermo Fisher). Then, B16F10 cells were opsonized with 10 μg/mL TA99 antibody (Genmab) for 30 min at RT to enhance phagocytosis.[57] Next, M1 macrophages were co-cultured with the target cells in a 1:4 (E:T) ratio for 4 h at 37°C and 5% CO_2. Finally, phagocytic uptake was determined by quantifying the percentage of CFSE$^+$ macrophages out of total F4/80$^+$ BMDMs using flow cytometry.

Generation and phagocytosis of human macrophages

CD14$^+$ PBMCs from buffy coats were isolated from complete PBMCs using an untouched pan monocyte isolation kit (Miltenyi Biotech) according to the manufacturers' protocol. These cells were then cultured for six days in standard IMDM, supplemented with 200 ng/mL GM-CSF (Immunotools). On day 4 of the culture, cells were additionally stimulated with 20 ng/mL IFN-γ (Peprotech) and 50 ng/mL LPS, resulting in M1-like macrophages. Then, cells were subjected to phagocytosis assays. Phagocytosis studies were performed similarly to BMDMs and BMDCs, with the exceptions that unstimulated K562.HLA-E$^+$ and K562.HLA-E$^-$ cells were used as target cells and CD47-blocking antibodies (10 μg/mL, Santa Cruz) were used to augment phagocytosis.[56] Phagocytic uptake was determined by quantifying the percentage of CFSE$^+$ macrophages out of total HLA-DR$^+$ macrophages using flow cytometry.

NK activation assay

Target cells were pre-stimulated (5 IU/mL IFN-γ for RAW264.7 cells, or 30 IU/mL IFN-γ and 10,000 IU/mL IFN-α for A20 cells) for two days. NK cells were obtained from spleens of naive C57BL/6 mice using a magnisort mouse NK cell enrichment kit (Invitrogen) according to the manufacturer's protocol. Then, NK cells (containing both NKG2A$^+$ and NKG2A$^-$ cells) and target cells were co-cultured at a 1:1 ratio for 6 h at 37°C and 5% CO_2 in the presence of 1 μg/mL Golgi plug (BD Biosciences). Finally, NK cell activation was assessed using intracellular flow cytometry measuring IFN-γ and NKG2A to distinguish between the activation of the two different subsets. To calculate the percentages of inhibition, the percentage of IFN-γ$^+$ NK cells from the various conditions were used as follows: ((RAW264.7 NKG2A$^+$ - medium NKG2A$^+$) – (RAW264.7 NKG2A$^-$ - medium NKG2A$^-$))/(RAW264.7 NKG2A$^+$ - medium NKG2A$^+$).

Surface protein stability assays

For the MHC-I stability assays in the presence of inhibitors, B16F10 or RAW264.7 cells were stimulated for 48 h with 30 IU/mL or 5 IU/mL IFN-γ, respectively. Then, the cells were harvested, divided over 15 mL tubes and cultured for a total of 6 h at 37°C and 5% CO_2 under constant rotation in a HulaMixer (Invitrogen) to keep the cells in suspension. After 3h, 5h, 5h 30 min, 5h 45 min, or 6h 1 μg/mL BFA, 50 μg/mL cycloheximide (Sigma-Aldrich), 1 μg/mL cytochalasin-D (Sigma-Aldrich), 150 nM marizomib (MedChemExpress), or combinations thereof were added to the culture. Then cells were stained at the same time point measuring Qa-1^b (6A8 antibody), Qdm/Qa-1^b (EXX1 antibody), H-2D^b (28.14.8S antibody) and PD-L1 (MIH5 antibody) and analyzed using flow cytometry.

The activity of cytochalasin-D was assessed by culturing IFN-γ pretreated RAW264.7 macrophages for 6 h with 25 μg/mL Sulforhodamine 101 (SR101, Sigma-Aldrich) fluorescent dye in the presence of 1 μg/mL cytochalasin-D. Uptake of SR101 was then quantified using flow cytometry.

Genome-wide CRISPR knockout screen for 6A8 and EXX1 binding

For knockout screening in the RAW264.7 cells, the mouse CRISPR Brie genome-wide knockout library was provided by David Root and John Doench. For virus production, HEK 293T cells were transfected with packaging plasmids pMDLg/pRRE (Addgene), pRSV-Rev (Addgene), pCMV-VSV-G (Addgene) together with the Brie plasmid using polyethyleneimine (Polyscience Inc.). Virus was harvested, filtered and 150 million RAW264.7 cells were transduced in the presence of 8 μg/mL polybrene (Millipore) at a multiplicity of infection (MOI) of 0.3. Transduced cells were selected using puromycin (2 μg/mL, Thermo Fisher) and after seven days, 50 million cells were stained for surface Qa-1^{b} or EXX1, and the lowest 5% of expressing cells were sorted using an Aria cell sorter (BD Biosciences). Cells were grown out and sorted again using the same gating as for the first sort. After this sort, genomic DNA (gDNA) was isolated using an isolate II genomic DNA kit (GC Biotech) for both the unsorted and sorted populations and gDNAs were amplified by PCR using a mix of forward primers and a specific barcoded KO reverse primer (included in Table S5 as NGS-Lib primers) for each sort and control.[97] gRNAs were sequenced using a NovaSeq600 system (Illumina) and inserts were mapped to the reference. Analysis of gRNA enrichment was done using PinAPL-Py.[98]

Genome-wide CRISPR activation screen for HLA-E binding

For CRISPRa screening for transmembrane interactors of HLA-E, K562 cells were transduced with dCAS-VP64_Blast and the genome-wide Calabrese activation library (sublibrary A + B), kindly provided by John Doench. Transduced cells were selected using blasticidin (5 μg/mL) and puromycin (2 μg/mL) and after seven days, two batches of 50 million cells were stained with a pool of four different HLA-E tetramers (VMAPRTLIL, RMPPLGHEL, RLPAKAPLL and VLRPGGHFL peptides, of which the latter three are known HLA-E binders from *mycobacterium tuberculosis*[99]) coupled to PE. Cells that stained positive for HLA-E PE (between 0.01 and 0.1%) were sorted using an Aria cell sorter and genomic DNA was isolated from the tetramer-positive and unsorted cells. gDNAs were amplified as above and sequenced using the Ilumina NovaSeq6000. Inserts were mapped to the reference and analysis of gRNA enrichment was done using PinAPL-Py.

LILRB1 reporter and adhesion assays

For reporter assays, 2B4-LILRB1 reporter cells were kindly provided by Dr. M. López Botet.[100] Reporter activation assays were performed by co-culturing 3 × 10^4 2B4-LILRB1 cells together with 6 × 10^4 Raji cells in a 1:2 ratio in a 96-well round bottom culture plate. Cells were harvested after 4h and GFP^{+} 2B4-LILRB1 reporter cells were quantified using flow cytometry.

For cell adhesion assays, Raji cells were incubated for 10 min with Celltrace Far Red (Thermo Fisher) and washed 2 times with PBS. Adhesion assays were performed by co-culturing 3 × 10^4 J774 cells with 9 × 10^4 Raji cells in a 1:3 ratio in an ultra-low attachment microplate 96-well (Corning) for 3h. Cells were then washed, and stained for H-2K^{d} (Bio-legend). After three PBS washes, double-positive H-2K^{d+} and Celltrace Far Red^{+} cells were quantified using flow cytometry without removing doublets, meaning these double-positive cells might result from both adhesion and phagocytosis.

Co-immunoprecipitations

To detect the HLA-E interaction with LILRB1 *in vitro*, 0.5 μg LILRB1-Fc (Sino Biological) was incubated in NP-40 buffer (0.5% NP-40 (Merck Millipore), 150 mM NaCl (VWR), 5 mM $MgCl_2$ (Sigma-Aldrich) and protease inhibitors (Roche)) at RT for 30 min with 0.5 μg HLA-E tetramer loaded with the indicated peptide. Subsequently, LILRB1-Fc was immunoprecipitated using Protein G Sepharose 4 FF beads (Sigma-Aldrich). Beads were washed 4x with NP-40 buffer, after which SDS-sample buffer (2% SDS (BioSolve), 10% glycerol (Sigma-Aldrich), 5% β-mercaptoethanol (Sigma-Aldrich), 60 mM Tris-HCl (Combi Blocks) pH 6.8 and 0.01% bromophenol blue (Merck)) was added to the beads. Samples were boiled before loading and proteins were separated by SDS-PAGE and transferred to Nitrocellulose filters (Cytiva). Blocking of the filter and antibody incubations was done in PBS supplemented with 0.1% (V/V) Tween 20 (Sigma-Aldrich) and 5% (W/V) milk powder (Sigma-Aldrich). Blots were stained using streptavidin 800 (LI-COR) and anti-human Fc 680 (LI-COR) and imaged using the Odyssey Imaging System (LI-COR).

Quantitative rt-PCR

Total RNA from B16, RAW264.7 and A20 cells was isolated using the Nucleospin RNA Plus kit (Macherey-Nagel) according to the manufacturers' protocol, with the exception that the cell pellets were vortexed for 30s to further facilitate cell lysis. cDNA was generated from the isolated RNA using the High-Capacity RNA-to-cDNA kit (ThermoFisher Scientific) according to the manufacturer's protocol with a starting concentration of 0.5 μg per reaction. Next, a qPCR mastermix was prepared in nuclease free water (in house pharmacy) containing 1–2 ng cDNA, iQ Sybr Green Supermix (Bio-Rad) and qPCR primers (Sigma-Aldrich, shown in resources table). Finally, the mix was added to a 384 well PCR plate (Bio-Rad), sealed with microseal B (Bio-Rad) and the plate was run on a CFX96 Real-Time PCR Detection System (Bio-Rad) using the following settings: 1) 95°C for 3 min, 2) 96°C for 10 s, 3) 60°C for 30 s + plate read, 4) repeat step 2 and 3 39 times, 5) 95°C for 10 s, 6) melt curve 65°C–95°C, increment 0.2°C, 10 s + plate read. The gene expression was normalized to the GAPDH housekeeping gene and the effect of IFN-γ was calculated from the difference in Cq between the

stimulated and unstimulated condition (ΔΔCq). For comparison of the baseline gene expression of RAW264.7 and A20 to B16, the normalized gene expression to GAPDH (ΔCq) for A20 and RAW264.7 was divided by the normalized gene expression to GAPDH for B16F10.

Mouse experiments

For analysis of Qdm/Qa-1^b expression in mice following administration of immunostimulatory agents, naive C57BL/6 mice were either injected with 30 mg/kg tilorone dihydrochloride (Sigma-Aldrich) i.p. and sacrificed after 24 h, or they were injected with 100 μg agonistic anti-CD40 antibody (clone FGK) i.v. on day 0 and day 1 and sacrificed on day 3.

For analysis of Qdm/Qa-1^b expression in the tumor microenvironment of mice, naive male C57BL/6 mice were inoculated with 100.000 B16F10 tumor cells s.c. in the flank on day 0. On day 6, lymphocytes from spleens and lymph nodes of naive TCR-transgenic pmel mice were isolated and enriched for T lymphocytes by nylon wool. 1 × 10^6 Enriched T cells were transferred by i.v. injection into the tail vein in 200 μL PBS. On day 7 and 14, mice were anesthetized by an i.p. injection of a mixture of ketamine (Alfasan) and xylazine (Dechra) and then immunized with 150 μg gp100$_{20–39}$ peptide (AVGALKVPRNQDWLGVPRQL homologous human sequence) in 100 μL PBS s.c. in the contralateral flank. As adjuvant, 60 mg of 5% imiquimod-containing cream Aldara (3M Pharmaceuticals) was simultaneously topically applied on the skin at the injection site. Recombinant human IL-2 (600,000 IU, Proleukin, Clinigen) was injected i.p. in 100 μL PBS at the end of day 14 and in the morning of day 15. Mice were sacrificed on day 20 and tissues were isolated for analysis by flow cytometry. Alternatively, naive female C57BL/6 mice were inoculated with 100.000 TC1 tumor cells s.c. in the flank on day 0. On day 8, the mice were immunized with 200 μg HPV16 E7$_{43-77}$ peptide (GQAEPDRAHYNIVTF CCKCDSTLRLCVQSTHVDIR) and 27μg CpG (ODN-1826, Invivogen) as an adjuvant in 100 μL PBS s.c. in the contralateral flank. Mice were sacrificed on day 18 and tissues were isolated for analysis by flow cytometry.

For therapeutic treatment with the EXX1 antibody, naive BALB/c mice were inoculated with 5 × 10^6 A20-eGFP/Fluc tumor cells as a mixture of 100 μL DPBS +0.1% BSA and 100 μL matrigel (Millipore-Sigma) s.c. in the flank on day 0. Tumors were measured three times a week with a VINCA DCLA-0605 digital caliper with tumor volume calculated as ((length x width^2)/2). When tumors were palpable (∼60mm^3), mice were randomized into treatment groups based on tumor volumes. Then, mice were treated with 200 μg EXX1 or isotype control antibodies i.p. in PBS on day 9, 11, 13, 15, 17 and 19. Mice were sacrificed when tumors reached a volume of 1500 mm^3.

QUANTIFICATION AND STATISTICAL ANALYSIS

All mouse experiments were performed with a minimum of three biological replicates. *In vitro* experiments were at least performed two times. Statistical tests are described in the figure legend, and calculated between two groups using an unpaired two-tailed student's t-test and between more than two groups using an ANOVA with Tukey's post-hoc test, unless otherwise indicated. Survival analyses were performed using a log rank Mantel-Cox test. GraphPad Prism (V9.2.0) was used for all statistical testing. Data are represented as mean ± SD unless indicated otherwise. Statistical significance is shown as *$p < 0.05$, **$p < 0.01$, ***$p < 0.001$ and ****$p < 0.0001$.

ADDITIONAL RESOURCES

There are no additional resources to report for this study.